High-accuracy Positioning Services for High-Speed Vehicles in Wideband mmWave Communications

Zijun Gong, *Member, IEEE*, Xuemin (Sherman) Shen, *Fellow, IEEE*, Cheng Li, *Senior Member, IEEE*, Yuhui Song, *Student Member, IEEE*, and Ruoyu Su, *Member, IEEE*

***Abstract*—It is expected that the sixth-generation (6G) cellular networks will provide high-accuracy positioning services. For the millimeter wave (mmWave) frequency band in 6G, both the Doppler and the spatial wideband effects can lead to channel variation in time and space domains, respectively. However, the impact of these effects on the positioning performance is not well studied. In this paper, we will investigate this issue and show that these two effects are not only challenges, but also provide great opportunities in terms of positioning in vehicular networks. Particularly, we will conduct system modeling, algorithm design, and fundamental performance analysis of simultaneous localization and communications (SLAC) in mmWave-based vehicular networks, exclusively dependent on channel state information. The major challenge in algorithm design is the high computational complexity that comes with the huge antenna arrays and bandwidth. For high-speed vehicle positioning, timeliness is as important as accuracy. For performance evaluation, the Cramér-Rao lower bounds (CRLB) will be derived as benchmarks. We will show that it is possible to achieve CRLB-level positioning accuracy, with almost linear complexity. With the closed-form theoretical results, we will evaluate how different system parameters contribute to positioning accuracy, such as bandwidth, carrier frequency, size and orientation of antenna arrays, etc. These results will shed light on system-level design and optimization of SLAC with ultra-wide frequency band in highly dynamic environments, i.e., very strong spatial wideband and Doppler effects. Comprehensive numerical results will also be presented to verify the theoretical analyses and the effectiveness of the proposed algorithms.**

***Index Terms*—Localization, ultra-wideband, millimeter wave; Doppler effect; beam squint; high-speed vehicles.**

I. Introduction

The real-time tracking of high-speed vehicles is a challenging problem, especially for bullet trains moving at a speed over 300 km/h. Over the past two decades, the Global Positioning System (GPS) has been playing a dominant role in providing outdoor positioning services. However, it has poor coverage in urban environments due to blockage, and very low refresh rate. With the advent of millimeter wave (mmWave) communications and massive MIMO (Multiple-Input-Multiple-Output) in the fifth- and sixth-generation (5G, 6G) cellular systems, we have another possible choice: the simultaneous localization and communications (SLAC) technique [1], [2]. SLAC will be able to provide ubiquitous positioning services, for both indoor and outdoor applications [3]. Compared with the GPS, SLAC has higher refresh rate, much improved coverage, and better accuracy. Meanwhile, the position information of the mobile devices helps to improve the communication performance [4]–[7]. For example, with location information, we can dynamically adjust the transmit powers of devices to guarantee the quality of service with minimum energy consumption [8]. With position information, a mobile device can quickly associate with base stations (BS) in its communication range [9]. In a wireless network, the position information of neighbour nodes can significantly improve the efficiency of routing protocols [10].

The idea of integrating positioning service into cellular communications is not new. In the era of the third-generation (3G) cellular communications, researchers have been talking about exploiting the huge bandwidth of CDMA (Code Division Multiple Access) for positioning [11]. Starting from the forth-generation (4G) cellular communications, i.e., Long Term Evolution (LTE), it has been shown that high-accuracy ranging can be achieved in OFDM systems [12]. The underlining idea is that the propagation delay will introduce a constant phase shift between adjacent sub-carriers. In 5G and 6G, the same MIMO-OFDM architecture will be employed for the physical layer, with two fundamental changes. First, the maximum number of antennas on a BS is eight in LTE, while hundreds of antennas are expected on 5G/6G BSs, referred to as massive MIMO [13], [14]. Second, the carrier frequency will be moved to the mmWave band, which brings much larger bandwidth. With the huge bandwidth and antenna arrays at the BS, we will be able to estimate the position of high-speed vehicles quickly and accurately [15]. In the recent 3GPP (Third Generation Partnership Project) release, the potential has been thoroughly investigated [16]. This technique is very promising because both the position and velocity information can be derived from the channel state information (CSI), which is readily available in mmWave communications. From the CSI, we can infer time of arrival (ToA), time difference of arrival (TDoA), angle of arrival (AoA), angle of departure (AoD), Doppler shift and received signal strength (RSS), etc. These parameters are strongly correlated to the positions and velocities of mobile devices.

To integrate localization into communications, there are several important research problems we need to consider: mitigation/utilization of multi-path components; single or multiple BS-based positioning; up-link/down-link pilot design for

Z. Gong is with the IOT Thrust, HKUST (Guangzhou), Guangzhou, China; and the Department of ECE, HKUST, Hong Kong SAR, China. He was an NSERC PDF at University of Waterloo with Prof. Shen (gongzijun@ust.hk).

Prof. X. (Sherman) Shen is with the Department of Electrical and Computer Engineering, University of Waterloo, Waterloo, ON, N2L 3G1, Canada (E-mail: sshen@uwaterloo.ca).

Prof. C. Li and Y. Song are with the Faculty of Engineering and Applied Science, Memorial University of Newfoundland, St. John's, NL, A1B 3X5, Canada (E-mail: (licheng,yuhuis)@mun.ca).

R. Su is with the School of Internet of Things, Nanjing University of Posts and Telecommunications, Nanjing, Jiangsu 210003, China (E-mail: suruoyu@njupt.edu.cn).

positioning. In the following section, existing work on these topics will be summarized.

II. Related Work

A. Multi-path: Foe or Friend?

For both wireless communications and geometry-based localization, such as triangulation and trilateration, an immediate problem is the multi-path effect. In wireless communications, the multi-path effect was viewed as interference in the first and second generation cellular communications. Starting from the 3G, people realized that the multi-path components (MPCs) can be harnessed to improve the signal to noise ratio (SNR), i.e., power gain of the Rake receivers. In the age of 4G, through the MIMO-OFDM architecture, we took one more step and started to utilize the multi-path effect to transmit multiple data streams simultaneously, i.e., the multiplexing gain! The multi-path effect has been turned from a foe to a friend in wireless communications. For localization, we witnessed a similar process.

In early research work on localization, the MPCs were viewed as interference, and only the line-of-sight (LoS) signal was believed to contain the mobile devices' position information [17]–[19], [19]. The GPS and radar are good examples of LoS-based positioning techniques. During the past two decades, the fundamental impacts of MPCs have been thoroughly investigated for different scenarios. Now we understand that MPCs can be a foe or friend, depending on the bandwidth and antenna configuration in geometry-based localization systems [20].

For single-input-single-output (SISO) systems, the MPCs will generally deteriorate positioning accuracy, suppose no prior information of the electromagnetic (EM) environment is available. However, if antenna arrays are available at both sides, i.e., MIMO, MPCs can directly help to improve positioning accuracy, as has been proved in [5] and [21]. Specifically, the authors of [21] pointed out that the MPCs will contribute to the positioning accuracy from two perspectives. On one perspective, each extra path will bring new information, concerning the mobile device's position. On the other hand, the extra path is always contaminated by noise, leading to position ambiguity/uncertainty. For wideband communications systems with large antenna arrays on both sides, the new information outweighs the concomitant uncertainty, leading to better positioning accuracy. In [22], the authors took one more step to show that the position and orientation tracking can be conducted with just one base station, based on discrete lens antenna arrays. It should be noted that only the LoS path can be used for tracking, because it is stable, while the reflected paths are not.

What if we have single-antenna mobile devices, i.e., multiple-input-single-output (MISO)? The SLAC based on single-antenna mobile devices is of great interest [2], [23], [24], because most small mobile devices are not equipped with massive arrays, especially in the future Internet of Things (IoT). Besides, even when they are equipped with small arrays, a MIMO system is equivalent to a MISO system if no CSI feedback link is available [25]. In such cases, the small array at the mobile device is only used to boost SNR. Both [2] and [24] consider single-antenna receivers in SLAC, and the authors showed that positioning accuracy will not benefit from the MPCs in such cases. As a matter of fact, when MPCs are not orthogonal with the LoS path signal, they will always deteriorate localization performance. Fortunately, with increased bandwidth and antenna array size, the MPCs will be asymptotically orthogonal to the LoS signal. In [26], the authors showed that MPCs can be ignored when the antenna arrays are large enough. A continuous bandwidth of 1 MHz was considered, and the authors showed that even for small antenna arrays, i.e., four at the transmitter and eight at the receiver, the multi-path effect can be ignored.

B. One or Multiple BSs?

The localization can be based on one or multiple BSs. For the cellular networks, single BS-based localization is more natural, because each mobile device is generally associated with only one BS at a time. However, poor accuracy is expected due to the limited bandwidth, and we need to take measures such as allowing mobile devices to share information with each other [27]. For example in [27], different single-antenna mobile devices are allowed to estimate mutual distances, and only AoA is estimated from the BS. In the era of 5G/6G, single BS-based localization becomes more reliable because the mobile devices can get multiple position-related measurements, including ToA, AoD and AoA. In [21], by measuring the ToA, AoD and AoA, a mobile device can localize itself with just one BS. In [28], the authors proposed a localization system based on only one BS with an antenna array. The antenna spacing is larger than half the wavelength, which brings higher spatial resolution and the necessity of phase unwrapping.

Localization based on distributed BSs is also becoming very popular in recent years. To understand this, note that blockage is a huge problem in mmWave communications. Therefore, a mobile device will generally maintain connections to multiple BSs simultaneously, i.e., multi-connectivity [7], [29]–[32]. For multiple BSs-based positioning, direct position determination (DPD) should be considered. In the conventional two-step localization, the intermediate parameters, such as AoA, ToA, TDoA and Doppler shift must be estimated in the first step. Then, these estimated parameters will be employed for localization in the second step. In the first step, different BSs are estimating these parameters independently, by ignoring their strong inherent correlations. Therefore, information loss is inevitable. With lower SNR, the information loss will be quite significant. To solve this issue, the DPD method was proposed in [33], [34], for narrow-band and wideband systems, respectively.

The DPD technique has been widely explored in SLAC. In [19], 2D direct localization was conducted without estimating the AoAs or delays. In [26], the authors proposed a DPD algorithm to combat the multi-path effect. The maximum likelihood estimate of a mobile device's position is directly extracted from the received waveforms. In [35], narrow-band training signals were employed for positioning, and a DPD

algorithm was proposed. To reduce the computational and communication overhead, the authors projected the received signals onto beamspace (i.e. the space domain). They showed that this can be done without information loss, by properly choosing the beamspace basis. In [36], a narrow-band model with phase noise at antennas was considered. From the estimated CSI, the authors dynamically adjust the sampling grid in space, to reduce the location quantization error. The joint channel estimation and localization was modelled as a unified sparse representation and recovery problem.

C. Down-link or Up-link?

For channel estimation, up-link (UL) training sequences are generally employed in time division duplex (TDD) systems [13]. The reason is that the training overhead is proportional to the number of transmit antennas, and the antenna array at BS is much larger than that on mobile devices. Then, the DL CSI can be derived from that of the UL by channel reciprocity [13]. For UL-based positioning, no additional overhead is required and the position information is just a byproduct of channel estimation [37]. As a result, positioning with UL signals is a more efficient and thus more common choice. However, the idea of DL signal-based positioning is also widely discussed [1], [2], [23], [24]. The motivations include improved energy efficiency on mobile devices, distribution of localization tasks, boosted SNR, improved security. In [38], the authors showed that covert localization is possible in wireless networks, and the security issue for UL-based positioning is not a big problem.

For DL-based SLAC, the needs of both localization and communications should be considered during beamforming. In [1], this problem was discussed, and the authors also took imperfect CSI and finite resolution of analog-to-digital-converter (ADC) into consideration. The channel estimation is conducted at the BS with UL training sequences, while the positioning is done at the mobile user side, after DL beamforming. Every mobile device can communicate with multiple BSs simultaneously, on different frequency bands. Therefore, a mobile device can receive DL signals from multiple BSs for self-positioning. In 3GPP Release 16, both UL and DL positioning signals are considered and numerical results can be found in [15]. For DL-based positioning with multiple BSs, different BSs will work on orthogonal time-frequency resources to avoid mutual interference.

From the above discussions, we can see that there are diverse research going on in SLAC, and many important questions concerning how SLAC systems should be designed have not been answered. In this paper, we will focus on SLAC systems based on single BS, high-mobility vehicles with single antenna, large antenna arrays on the BS, and huge bandwidth on mmWave band. In such cases, the beam squint and Doppler effect must be considered [39], [40]. Beam squint is also referred to as the spatial wideband effect, with which different sub-carriers will have different spatial signatures. We will conduct comprehensive system modeling, algorithm design, and performance analysis for the above mentioned SLAC systems. An uniform planar array (UPA) is considered on the BS side, because it can be used to estimate both the azimuth and elevation angles. Compared with existing work, our major contributions are summarized below.

- The spatial wideband effect (beam squint) is considered in modeling, and its impact on positioning accuracy is quantified. We will see that ignoring this effect will lead to huge angle estimation error. A sub-optimal low-complexity algorithm is proposed to solve this problem, and shown to closely approximate the CRLB.
- The Doppler effect has been viewed as a challenge in communications, especially for high-frequency mmWave signals and high-speed vehicles. However, we will see that the Doppler shifts also contain mobile device's position information, and this information can be extracted if map of the target area is available.
- The orientation and position of the antenna array at the BS are very important for positioning. We will show that the elevation plays a dominant role, while the impact of azimuth is negligible. A very simple equation is derived for orientation optimization and shown to be very accurate.

The remaining parts of this paper are organized as follows. In Section III, the channel model is presented, considering the beam squint and Doppler effects. In Section IV, the Cramér-Rao lower bound (CRLB) is derived for different scenarios, and the impacts of the beam squint and Doppler effect on positioning accuracy are quantified. Based on this model, low-complexity algorithms are presented for parameter estimation and localization in Section V. Following that, numerical results can be found in Section VI. The last section concludes this paper and lists several potential research directions for future work.

Notations: throughout this paper, the upper case bold letters represent matrixes while the lower case bold font denotes column vectors. For an arbitrary vector $\mathbf{a}$, $\mathbf{a}[n]$ is the n-th element. $\mathbf{A}^T$, $\mathbf{A}^H$, and $\mathbf{A}^*$ indicate the transpose, Hermitian transpose, and element-wise conjugate of matrix $\mathbf{A}$. $\|\cdot\|$ denotes the L_2 norm of a vector, while $\|\cdot\|_F$ denotes the Frobenius norm of a matrix. $\mathrm{tr}\{\mathbf{A}\}$ gives the trace of matrix $\mathbf{A}$. $\mathrm{diag}\{\mathbf{A}\}$ gives a column vector containing the diagonal elements of $\mathbf{A}$, while $\mathrm{diag}\{\mathbf{a}\}$ constructs a diagonal matrix with elements of $\mathbf{a}$.

III. System Modeling

Consider wideband mmWave communications between single-antenna vehicles and a BS equipped with a UPA. The classic MIMO-OFDM structure is employed to combat the wideband effect (inter-symbol-interference in time domain), and suppose we have N_s sub-carriers, with a sub-carrier spacing of B Hz. The n_s-th sub-carrier has a central frequency of $f_{n_s} = f_0 + n_s B$, $(n_s \in \{0, 1, \cdots, N_s - 1\})$, with f_0 being the frequency of the 0-th sub-carrier. Suppose the carrier frequency is f_c, and we have $f_c = f_0 + (N_s - 1)B/2$. Consider an UPA with $N_x \times N_y$ antennas at the BS, and the distance between adjacent antennas is D in both directions. Without loss of generality, we build a three dimensional (3D) right-handed coordinate system with the origin at the (0,0)-th

antenna. The coordinate of the (n_x, n_y)-th antenna element is $\mathbf{x}_{n_x,n_y} = [n_x D, n_y D, 0]^T$ (for $n_x \in \{0, 1, \cdots, N_x - 1\}$ and $n_y \in \{0, 1, \cdots, N_y - 1\}$). The vehicle is located at $\mathbf{x}(t) = \mathbf{x}_0 + \mathbf{v}t$ at time t, with $\mathbf{x}_0 = [x, y, z]^T$ being the initial position and $\mathbf{v}$ being the 3D velocity of the vehicle. In the following discussions, we will assume the vehicle has a constant velocity in one frame. The reason is that one frame is very short in wireless communications (e.g., 1 ms in LTE), and the velocity of a vehicle cannot change significantly in such a short period.

For a wireless channel with a propagation delay of τ seconds and a real channel gain of α, the equivalent baseband channel response is $\alpha e^{-j2\pi f\tau}$ for narrow-band signals, at frequency f. For wideband communications, the propagation delay will lead to different phase shifts on different frequencies. Therefore, at the n_t-th time slot, for the (n_x, n_y)-th antenna, the baseband equivalent channel gain on the n_s-th sub-carrier will be

$$h_{n_t,n_s,n_x,n_y} = \alpha \exp(-j2\pi f_{n_s} \tau_{n_x,n_y}(n_t T) + j\phi), \quad (1)$$

with $T = 1/B$ being the OFDM symbol duration and ϕ being a random phase disturbance. $\tau_{n_x,n_y}(n_t T)$ is the propagation delay from the vehicle to the (n_x, n_y)-th antenna on the BS at the n_t-th time slot. As we can see, the phase shift caused by the propagation delay is dependent on frequency, space (i.e., antenna index), and time.

In practice, the propagation delay varies over time, and it is generally nonlinear. To see this, we have the real-time distance of the (n_x, n_y)-th antenna and the vehicle at time t as

$$d_{n_x,n_y}(t) = \|\mathbf{x}_0 + \mathbf{v}t - \mathbf{x}_{n_x,n_y}\|. \quad (2)$$

In one data frame (one millisecond in LTE), we have $\|\mathbf{x}_{n_x,n_y}\| \ll \|\mathbf{x}_0\|$ and $\|\mathbf{v}t\| \ll \|\mathbf{x}_0\|$. Therefore, taking the first-order Taylor approximation, we obtain

$$d^{(1)}_{n_x,n_y}(t) = d_0 + \frac{\mathbf{x}_0^T \mathbf{v}}{d_0} t - \frac{\mathbf{x}_0^T \mathbf{x}_{n_x,n_y}}{d_0}, \quad (3)$$

with $d_0 = \|\mathbf{x}_0\|$. Suppose the angle between the moving direction of the vehicle (i.e., $\mathbf{v}$) and the vector pointing from the vehicle to the BS (i.e., $-\mathbf{x}_0$) is θ_v, we have $\mathbf{x}_0^T \mathbf{v}/d_0 = -\|\mathbf{v}\| \cos\theta_v$. Therefore, we can rewrite (3) as

$$d^{(1)}_{n_x,n_y}(t) = d_0 - \|\mathbf{v}\| \cos\theta_v t - n_x D \cos\theta_x - n_y D \cos\theta_y, \quad (4)$$

where θ_x and θ_y are the angles formed by $\mathbf{x}_0$ with the $+x$-axis and $+y$-axis, respectively. In this case, we have $\cos\theta_x = x/d_0$ and $\cos\theta_y = y/d_0$. The geometrical model of this system is presented in Fig. 1.

Then, we can approximate the propagation delay as $\tau_{n_x,n_y}(n_t T) \approx d^{(1)}_{n_x,n_y}(n_t T)/c$, and c is the speed of light. Without loss of generality, we assume the antennas are critically spaced in both directions, i.e., $D = \lambda_c/2$, and $\lambda_c = c/f_c$ is the wavelength of the carrier. To simplify the notations, we define

$$\begin{aligned} \omega_s &= 2\pi B d_0/c, \\ \omega_{x,n_s} &= -2\pi f_{n_s} D \cos\theta_x/c = \omega_x f_{n_s}/f_c, \\ \omega_{y,n_s} &= -2\pi f_{n_s} D \cos\theta_y/c = \omega_y f_{n_s}/f_c, \\ \omega_{t,n_s} &= 2\pi f_{n_s} v_r/B/c = \omega_t f_{n_s}, \end{aligned} \quad (5)$$

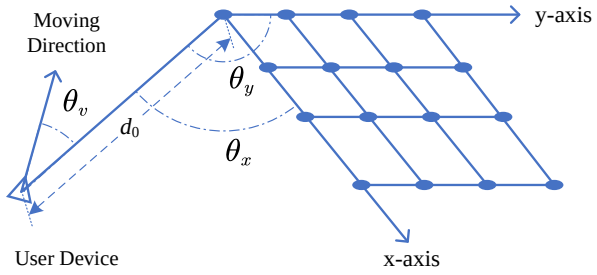

Fig. 1: Geometrical model of the system.

where $\omega_x = -\pi \cos\theta_x$, $\omega_y = -\pi \cos\theta_y$, $\omega_t = 2\pi v_r/B/c$ and $v_r = -\|\mathbf{v}\| \cos\theta_v$ is the radial velocity of the vehicle with respect to the BS. Then (1) can be rewritten as

$$h_{n_t,n_s,n_x,n_y} = \alpha e^{-j(n_s\omega_s + n_x\omega_{x,n_s} + n_y\omega_{y,n_s} + n_t\omega_{t,n_s} + \phi_0)}, \quad (6)$$

where $\phi_0 = 2\pi f_0 d_0/c - \phi$. Here, ω_{x,n_s} and ω_{y,n_s} are dependent on the AoA and sub-carrier index, and they are often referred to as spatial signatures of the received signals, because they have a one-to-one relation with the AoA, given that the antenna spacing is no larger than half the carrier wavelength [41]. In wideband communications, we can see that the spatial signatures on different sub-carriers are different, even for signal coming from the same direction, i.e., the spatial wideband effect, or beam squint effect. Similarly, ω_{t,n_s} is proportional to the radial velocity of the vehicle with respect to the BS, i.e, the Doppler effect, and it is also dependent on sub-carrier index, due to the wideband effect. Also, we can see that the phase difference between adjacent sub-carriers, i.e., ω_s, is proportional to the distance between vehicle and BS. By estimating these parameters, we can get d_0, θ_x, θ_y, v_r. These four parameters are directly related to the target's 3D coordinate and velocity, and positioning based on CSI is thus possible.

To summarize, what (6) tells us is that the geometrical channel parameters, including propagation delay, angle of arrival and Doppler shift, can all be observed on complex channel gains in the form of phase shift. For example, ω_s denotes the phase shift between adjacent sub-carriers, caused by propagation delay; ω_x is the phase shift between adjacent antennas on the x-axis, dependent on θ_x; ω_y is the phase shift between adjacent antennas on y-axis, dependent on θ_y; ω_t is the phase shift between adjacent time slots, resulting from the Doppler effect. However, note that the later three phase shifts are all dependent on the central frequency of the signal, which means they vary among sub-carrier, i.e., ω_{x,n_s}, ω_{y,n_s} and ω_{t,n_s}. To make it easier to follow, we summarized the important system parameters in Table I.

For notational convenience, we rewrite the array response at the n_s-th sub-carrier and the n_t-th time slot as

$$\mathbf{H}_{n_t,n_s}[n_x, n_y] = h_{n_t,n_s,n_x,n_y}. \quad (7)$$

As we can see, the array response varies with both time and frequency, caused by the Doppler effect and the beam squint,

TABLE I: Important Parameters

	Variable	Value
Sub-Carrier Index	n_s	0 to N_s-1
Time Index	n_t	0 to N_t-1
Antenna Index on x-axis	n_x	0 to N_x-1
Antenna Index on y-axis	n_y	0 to N_y-1
Phase Shift of Sub-carriers	ω_s	$[-\pi,\pi)$
Phase Shift of Time Slots	ω_t	$[-\pi,\pi)$
Phase Shift of Antennas on x-axis	ω_x	$[-\pi,\pi)$
Phase Shift of Antennas on y-axis	ω_y	$[-\pi,\pi)$

respectively. Furthermore, we define a N-dimensional steering vector as

$$\mathbf{a}_N(\omega)=\left[1,e^{-j\omega},e^{-j2\omega},\cdots,e^{-j(N-1)\omega}\right]^T. \tag{8}$$

Thus, $\mathbf{H}_{n_t,n_s}$ can be rewritten as $\mathbf{H}_{n_t,n_s}=\alpha_{n_t,n_s}\mathbf{a}_{N_x}(\omega_{x,n_s})\,\mathbf{a}_{N_y}^T(\omega_{y,n_s})$, where α_{n_t,n_s} is the complex channel gain on the n_s-th sub-carrier and n_t-th time slot, given as

$$\alpha_{n_t,n_s}=\alpha e^{-j(n_s\omega_s+n_t\omega_{t,n_s}+\phi_0)}. \tag{9}$$

In the following sections, based on this channel model, we will first analyze how different system parameters contribute to positioning accuracy by deriving the CRLB, and then talk about how the geometrical parameters can be estimated through low-complexity algorithms. Based on the estimated geometrical parameters, localization will then be conducted.

IV. CRLB Analysis

In mmWave-based SLAC, the positioning accuracy is impacted by many parameters, such as carrier frequency, bandwidth, sub-carrier spacing, frame length, antenna array size, etc. Meanwhile, the relative position and velocity between the BS and a mobile device also strongly affect positioning accuracy. In system optimization and algorithm design, it is very important to understand how different system parameters contribute to positioning accuracy. In this section, we will derive the CRLB, and use it as a benchmark for performance analysis. By doing so, we will be able to answer some fundamental questions. For example, how does the orientation of the antenna array contribute to positioning accuracy, and how should we place the array for optimal performance? Will the Doppler shift measurements help to improve positioning accuracy? Does the spatial wideband effect necessarily deteriorate system performance?

To start with, we will first analyze the channel estimation accuracy in the following sub-section. The estimation error in channel parameters will lead to positioning error, and the connection will be unveiled in the second sub-section. In the third sub-section, we talk about how to optimize the orientation of the antenna array at the BS, while the last sub-section covers the impacts of the Doppler effect and beam squint.

A. Channel Estimation

In an arbitrary data frame, suppose s_{n_t,n_s} is the transmitted pilot symbol on the n_t-th time slot and n_s-th sub-carrier, which is known at the BS side.[1] The received signal at the BS will be

$$\mathbf{Y}_{n_t,n_s}=\mathbf{H}_{n_t,n_s}s_{n_t,n_s}+\mathbf{N}_{n_t,n_s}, \tag{10}$$

with $\mathbf{N}_{n_t,n_s}$ being additive white Gaussian noise. $\boldsymbol{\theta}=[\omega_s,\omega_x,\omega_y,\omega_t,\phi_0,\alpha]^T$ contains all the unknown channel parameters. Consider independent and identically distributed (i.i.d.) circularly symmetric complex Gaussian (CSCG) noise, the probability density function (PDF) of the received signal is

$$p_{n_t,n_s}(\mathbf{Y}_{n_t,n_s}|\boldsymbol{\theta})=\left(\pi\sigma^2\right)^{-N_xN_y}\exp\left(-\frac{\|\mathbf{Y}_{n_t,n_s}-s_{n_t,n_s}\mathbf{H}_{n_t,n_s}\|_F^2}{\sigma^2}\right), \tag{11}$$

where σ^2 is the variance of the noise components. The log-likelihood function will be

$$l_{n_t,n_s}(\mathbf{Y}_{n_t,n_s}|\boldsymbol{\theta})=\ln p_{n_t,n_s}(\mathbf{Y}_{n_t,n_s}|\boldsymbol{\theta}), \tag{12}$$

with $\ln(\cdot)$ denoting the natural logarithm. The Fisher information matrix (FIM) is thus given as

$$\mathbf{F}_{n_t,n_s}(\boldsymbol{\theta})=\mathbb{E}\left\{\nabla_{\boldsymbol{\theta}}l_{n_t,n_s}\nabla_{\boldsymbol{\theta}}^T l_{n_t,n_s}\right\}. \tag{13}$$

Through tedious but straight forward derivations, we can get the explicit expression of the FIM in (14) (at the top of the next page), where $\bar{n}_x=\frac{1}{N_x}\sum_{n_x}n_x$, $\overline{n_x^2}=\frac{1}{N_x}\sum_{n_x}n_x^2$, $\bar{n}_y=\frac{1}{N_y}\sum_{n_y}n_y$ and $\overline{n_y^2}=\frac{1}{N_y}\sum_{n_y}n_y^2$. E_{n_t,n_s} is the energy of s_{n_t,n_s}, i.e., $E_{n_t,n_s}=|s_{n_t,n_s}|^2$.

$\mathbf{F}_{n_t,n_s}(\boldsymbol{\theta})$ quantifies the amount of information concerning $\boldsymbol{\theta}$ that can be extracted from the CSI obtained at the n_s-th sub-carrier and n_t-th time slot. With all the information collected from different sub-carriers and time slots, we have the FIM with respect to $\boldsymbol{\theta}$ as

$$\mathbf{F}_{\boldsymbol{\theta}}=\sum_{n_t}\sum_{n_s}\mathbf{F}_{n_t,n_s}(\boldsymbol{\theta}). \tag{15}$$

Note that $\mathbf{F}_{\boldsymbol{\theta}}$ quantifies the amount of information in the least squares (LS) channel estimate concerning the channel parameters, i.e., $\boldsymbol{\theta}$. With different observations from various time slots and sub-carriers, we can extract more and more information, and they add up to $\mathbf{F}_{\boldsymbol{\theta}}$. The addition of information is rooted in the assumption of independent noise in different observations. In $\boldsymbol{\theta}$, we are particularly interested in the first three parameters, because they contain the position-related information. Therefore, we define $\boldsymbol{\omega}=\boldsymbol{\theta}[1:3]=[\omega_s,\omega_x,\omega_y]^T$. By deriving the CRLB of $\boldsymbol{\omega}$, we can have a rough idea about the achievable positioning accuracy. To simplify the notations, we define $\mathbf{A}=\mathbf{F}_{\boldsymbol{\theta}}[1:3,1:3]$, $\mathbf{B}=\mathbf{F}_{\boldsymbol{\theta}}[1:3,4:6]$, $\mathbf{C}=\mathbf{F}_{\boldsymbol{\theta}}[4:6,4:6]$. The CRLB of $\boldsymbol{\theta}$ will be

$$\mathbf{R}_{\boldsymbol{\theta}}=\mathbf{F}_{\boldsymbol{\theta}}^{-1}=\begin{bmatrix}\left(\mathbf{A}-\mathbf{B}\mathbf{C}^{-1}\mathbf{B}^T\right)^{-1} & \tilde{\mathbf{B}}\\ \tilde{\mathbf{B}}^T & \left(\mathbf{C}-\mathbf{B}^T\mathbf{A}^{-1}\mathbf{B}\right)^{-1}\end{bmatrix}, \tag{16}$$

[1] After initial channel estimation, we can use both the pilot symbols and data symbols for channel tracking, and thus vehicle's position tracking [25]. Without loss of generality, we assume sets $\mathcal{N}_t$ and $\mathcal{N}_s$ contain the indexes of time slots and sub-carriers employed for channel estimation, i.e., $n_t\in\mathcal{N}_t$ and $n_s\in\mathcal{N}_s$.

$$\mathbf{F}_{n_t,n_s}(\boldsymbol{\theta}) = \frac{2E_{n_t,n_s}\alpha^2 N_x N_y}{\sigma^2} \begin{bmatrix} n_s^2 & n_s\bar{n}_x\frac{f_{n_s}}{f_c} & n_s\bar{n}_y\frac{f_{n_s}}{f_c} & n_t n_s f_{n_s} & n_s & 0 \\ n_s\bar{n}_x\frac{f_{n_s}}{f_c} & \overline{n_x^2}\frac{f_{n_s}^2}{f_c^2} & \bar{n}_x\bar{n}_y\frac{f_{n_s}^2}{f_c^2} & n_t\bar{n}_x\frac{f_{n_s}^2}{f_c} & \bar{n}_x\frac{f_{n_s}}{f_c} & 0 \\ n_s\bar{n}_y\frac{f_{n_s}}{f_c} & \bar{n}_x\bar{n}_y\frac{f_{n_s}^2}{f_c^2} & \overline{n_y^2}\frac{f_{n_s}^2}{f_c^2} & n_t\bar{n}_y\frac{f_{n_s}^2}{f_c} & \frac{f_{n_s}}{f_c}\bar{n}_y & 0 \\ n_t n_s f_{n_s} & n_t\bar{n}_x\frac{f_{n_s}^2}{f_c} & n_t\bar{n}_y\frac{f_{n_s}^2}{f_c} & n_t^2 f_{n_s}^2 & n_t f_{n_s} & 0 \\ n_s & \bar{n}_x\frac{f_{n_s}}{f_c} & \bar{n}_y\frac{f_{n_s}}{f_c} & n_t f_{n_s} & 1 & 0 \\ 0 & 0 & 0 & 0 & 0 & 1/\alpha^2 \end{bmatrix} \tag{14}$$

with $\tilde{\mathbf{B}} = \left(\mathbf{A} - \mathbf{B}\mathbf{C}^{-1}\mathbf{B}^T\right)^{-1}\mathbf{B}\mathbf{C}^{-1}$. Then, we have the CRLB of $\boldsymbol{\omega}$ as

$$\mathbf{R}_{\boldsymbol{\omega}} = \mathbf{R}_{\boldsymbol{\theta}}[1:3,1:3] = \left(\mathbf{A} - \mathbf{B}\mathbf{C}^{-1}\mathbf{B}^T\right)^{-1}. \tag{17}$$

Suppose the CRLB of ω_s, ω_x and ω_y are $\sigma^2_{\omega_s}$, $\sigma^2_{\omega_x}$,$\sigma^2_{\omega_y}$, we have $\mathrm{diag}\{\mathbf{R}_{\boldsymbol{\omega}}\} = [\sigma^2_{\omega_s},\sigma^2_{\omega_x},\sigma^2_{\omega_y}]^T$. Note that ω_s is proportional to the propagation delay, and thus d_0. Therefore, the CRLB of ranging error is

$$\sigma^2_{d_0} = \sigma^2_{\omega_s}\left(\frac{c}{2\pi B}\right)^2. \tag{18}$$

B. CRLB of Positioning Error in One Frame

In the previous sub-section, we derived the CRLB of channel parameters, and in this sub-section we will derive that of the positioning error. Define $\boldsymbol{\eta} = [\mathbf{x}_0^T, v_r, \phi_0, \alpha]^T$, and the PDF of $\mathbf{Y}_{n_t,n_s}$ given $\boldsymbol{\eta}$ will be

$$p_{n_t,n_s}(\mathbf{Y}_{n_t,n_s}|\boldsymbol{\eta}) = p_{n_t,n_s}(\mathbf{Y}_{n_t,n_s}|\boldsymbol{\theta}), \tag{19}$$

because of the one-to-one relation between $\boldsymbol{\theta}$ and $\boldsymbol{\eta}$. There are totally six unknowns: the 3D coordinate and radial velocity of the vehicle, random phase shift and the real channel gain. In these six unknowns, we are particularly interested in the first four, i.e., the geometrical channel parameters. The log-likelihood function is

$$l_{n_t,n_s}(\mathbf{Y}_{n_t,n_s}|\boldsymbol{\eta}) = \ln p_{n_t,n_s}(\mathbf{Y}_{n_t,n_s}|\boldsymbol{\eta}), \tag{20}$$

and the FIM is then computed as

$$\mathbf{F}_{n_t,n_s}(\boldsymbol{\eta}) = \mathbb{E}\left\{\nabla_{\boldsymbol{\eta}} l_{n_t,n_s} \nabla_{\boldsymbol{\eta}}^T l_{n_t,n_s}\right\}. \tag{21}$$

During channel estimation and channel tracking, we will be estimating $\boldsymbol{\theta}$, based on which the position and velocity information can be extracted. Therefore, we are interested in how the FIM of channel estimation is related to that of positioning. To unveil the relation, we start with the chain rule:

$$\nabla_{\boldsymbol{\eta}} l_{n_t,n_s} = \nabla_{\boldsymbol{\eta}}^T\boldsymbol{\theta}\nabla_{\boldsymbol{\theta}} l_{n_t,n_s}. \tag{22}$$

By replacing $\nabla_{\boldsymbol{\eta}} l_{n_t,n_s}$ with the right hand side of (22), we can rewrite (21) as

$$\mathbf{F}_{n_t,n_s}(\boldsymbol{\eta}) = \nabla_{\boldsymbol{\eta}}^T\boldsymbol{\theta}\mathbf{F}_{n_t,n_s}(\boldsymbol{\theta})\nabla_{\boldsymbol{\eta}}\boldsymbol{\theta}. \tag{23}$$

Then we can add the information from different sub-carriers and time slots, leading to the FIM:

$$\mathbf{F}_{\boldsymbol{\eta}} = \sum_{n_t}\sum_{n_s}\mathbf{F}_{n_t,n_s}(\boldsymbol{\eta}) = \nabla_{\boldsymbol{\eta}}^T\boldsymbol{\theta}\mathbf{F}_{\boldsymbol{\theta}}\nabla_{\boldsymbol{\eta}}\boldsymbol{\theta}. \tag{24}$$

Notice that the Jacobian of $\boldsymbol{\theta}$ with respect to $\boldsymbol{\eta}$ is a block diagonal matrix:

$$\nabla_{\boldsymbol{\eta}}\boldsymbol{\theta} = \begin{bmatrix} \mathbf{P} & \mathbf{0} \\ \mathbf{0} & \mathbf{P}_0 \end{bmatrix}, \tag{25}$$

with $\mathbf{P}_0 = \mathrm{diag}\left\{\left[\frac{\partial\omega_t}{\partial v_r}, 1, 1\right]\right\}$ and $\mathbf{P}$ given as

$$\mathbf{P} = \begin{bmatrix} \frac{2\pi B}{c}\frac{x}{d_0} & \frac{2\pi B}{c}\frac{y}{d_0} & \frac{2\pi B}{c}\frac{z}{d_0} \\ -\pi\left(\frac{1}{d_0} - \frac{x^2}{d_0^3}\right) & \frac{\pi xy}{d_0^3} & \frac{\pi xz}{d_0^3} \\ \frac{\pi xy}{d_0^3} & -\pi\left(\frac{1}{d_0} - \frac{y^2}{d_0^3}\right) & \frac{\pi yz}{d_0^3} \end{bmatrix}. \tag{26}$$

The FIM of $\boldsymbol{\eta}$ can be written as

$$\mathbf{F}_{\boldsymbol{\eta}} = \begin{bmatrix} \mathbf{P}^T & \mathbf{0} \\ \mathbf{0} & \mathbf{P}_0^T \end{bmatrix}\begin{bmatrix} \mathbf{A} & \mathbf{B} \\ \mathbf{B}^T & \mathbf{C} \end{bmatrix}\begin{bmatrix} \mathbf{P} & \mathbf{0} \\ \mathbf{0} & \mathbf{P}_0 \end{bmatrix}. \tag{27}$$

The CRLB of $\boldsymbol{\eta}$ will be

$$\mathbf{R}_{\boldsymbol{\eta}} = \mathbf{F}_{\boldsymbol{\eta}}^{-1} = \begin{bmatrix} \mathbf{P}^{-1} & \mathbf{0} \\ \mathbf{0} & \mathbf{P}_0^{-1} \end{bmatrix}\mathbf{R}_{\boldsymbol{\theta}}\begin{bmatrix} \mathbf{P}^{-T} & \mathbf{0} \\ \mathbf{0} & \mathbf{P}_0^{-T} \end{bmatrix}. \tag{28}$$

The CRLB concerning $\mathbf{x}_0$ is thus

$$\mathbf{R}_{\mathbf{x}_0} = \mathbf{R}_{\boldsymbol{\eta}}[1:3,1:3] = \mathbf{P}^{-1}\mathbf{R}_{\boldsymbol{\omega}}\mathbf{P}^{-T}, \tag{29}$$

and the overall lower bound of mean square error (MSE) in 3D positioning will be

$$\sigma^2_{\mathbf{x}_0} = \mathrm{tr}\{\mathbf{R}_{\mathbf{x}_0}\}. \tag{30}$$

For the radial velocity, the CRLB is

$$R_{v_r} = \frac{4\pi^2}{B^2c^2}\left(\mathbf{C} - \mathbf{B}^T\mathbf{A}^{-1}\mathbf{B}\right)^{-1}[1,1]. \tag{31}$$

C. Orientation of the BS Array

In SLAC, the BS antenna array serves both communications and localization purposes. Intuitively, we need to optimize the orientation of the antenna array for both applications. However, from the previous analysis, we can see that the channel estimation accuracy is not dependent on geometrical relation between the transmitter and receiver. Therefore, only the minimization of the positioning error will be considered when we install the antenna array on the BS.

In (30), we can see that the positioning error is not only dependent on the orientation of the antenna array, but also the distance between the vehicle and the BS. The impacts of orientation and distance are coupled, i.e., for different distances, the optimal orientation is not fixed. However, we will see that the coupling is weak and the impacts of distance and orientation can be isolated through the following approximation.

In Appendix A, we showed that $\mathbf{P}$ can be decomposed as

$$\mathbf{P}^{-1} = -\frac{d_0}{\pi} \underbrace{\begin{bmatrix} 1 & 0 & -x/z \\ 0 & 1 & -y/z \\ -x/z & -y/z & -1 \end{bmatrix}}_{\mathbf{A_P}} \underbrace{\begin{bmatrix} 0 & 1 & 0 \\ 0 & 0 & 1 \\ \frac{cz}{2Bd_0^2} & 0 & 0 \end{bmatrix}}_{\mathbf{D_P}}. \tag{32}$$

As shown in (32), we define these two matrixes on the right hand side as $\mathbf{A_P}$ and $\mathbf{D_P}$, respectively. The covariance matrix of $\mathbf{x}_0$ can be rewritten as

$$\mathbf{R}_{\mathbf{x}_0} = \frac{d_0^2}{\pi^2} \mathbf{A_P} \mathbf{D_P} \mathbf{R}_{\boldsymbol{\omega}} \mathbf{D}_{\mathbf{P}}^T \mathbf{A_P}. \tag{33}$$

The variance of positioning error is

$$\sigma_{\mathbf{x}_0}^2 = \frac{d_0^2}{\pi^2} \operatorname{tr}\{\mathbf{D_P} \mathbf{R}_{\boldsymbol{\omega}} \mathbf{D}_{\mathbf{P}}^T \mathbf{A}_{\mathbf{P}}^2\}. \tag{34}$$

The off-diagonal elements in $\mathbf{R}_{\boldsymbol{\omega}}$ are much smaller than the diagonal ones, and we approximately have

$$\sigma_{\mathbf{x}_0}^2 \approx \frac{d_0^2}{\pi^2} \operatorname{tr}\{\mathbf{D_P} \operatorname{diag}\{\mathbf{R}_{\boldsymbol{\omega}}\} \mathbf{D}_{\mathbf{P}}^T \mathbf{A}_{\mathbf{P}}^2\}. \tag{35}$$

It can be easily verified that $\mathbf{D_P} \operatorname{diag}\{\mathbf{R}_{\boldsymbol{\omega}}\} \mathbf{D}_{\mathbf{P}}^T$ is diagonal, given by

$$\mathbf{D_P} \operatorname{diag}\{\mathbf{R}_{\boldsymbol{\omega}}\} \mathbf{D}_{\mathbf{P}}^T = \operatorname{diag}\{\mathbf{R}_{\boldsymbol{\omega}}\} \operatorname{diag}\left\{1, 1, \left(\frac{cz}{2Bd_0^2}\right)^2\right\}. \tag{36}$$

Furthermore, suppose θ_z is the angle formed by the signal's AoA and the $+z$ axis, i.e., $\cos\theta_z = z/d_0$, and the corresponding spatial signature is $\omega_z = -\pi\cos\theta_z$. Then, the lower bound of positioning error can be approximated by

$$\sigma_{\mathbf{x}_0}^2 \approx \frac{d_0^2}{\pi^2} \left(\left(1 + \frac{\omega_x^2}{\omega_z^2}\right) \sigma_{\omega_x}^2 + \left(1 + \frac{\omega_y^2}{\omega_z^2}\right) \sigma_{\omega_y}^2 \right) + \sigma_{d_0}^2. \tag{37}$$

Note that $\sigma_{\omega_x}^2$, $\sigma_{\omega_y}^2$ and $\sigma_{d_0}^2$ are not dependent on the antenna array's orientation. Besides, the angle θ_z is not the *elevation*, and the elevation is the angle formed by the signal's AoA with the xy-plane, given as $\pi/2 - \theta_z$.

From this simplified equation, we first notice that the positioning error contains two parts. The second part is the constant ranging error, while the first part is proportional to the distance between BS and vehicle. By properly choosing the orientation of the antenna array, we can adjust ω_x, ω_y and ω_z to minimize the first part. For the given coverage area, we want to minimize the maximum positioning error. In this case, we need to conduct optimization over both elevation and azimuth. However, we will see that elevation dominates the positioning error.

When $N_x = N_y$, we have $\sigma_{\omega_x} = \sigma_{\omega_y}$, i.e., equal AoA estimation error on x- and y-directions. In this case, we can further simplify (37) as

$$\sigma_{\mathbf{x}_0}^2 \approx d_0^2 \left(1 + \pi^2/\omega_z^2\right) \sigma_{\omega_x}^2 + \sigma_{d_0}^2, \tag{38}$$

where we implicitly used the fact that $\omega_x^2 + \omega_y^2 + \omega_z^2 = \pi^2$. In this case, we can more clearly see that the elevation (i.e., $\pi/2 - \theta_z$) is critical for positioning precision. When elevation is close to $\pi/2$ (or θ_z close to 0), the positioning error is minimized. Fig. 2 shows that this approximation is very accurate. In Fig. 2, the parentheses indicate units, while the forward slash means division or normalization. In this figure particularly, the forward slash means normalizing the elevation by π. For every given elevation (or θ_z), the positioning error is dependent on the azimuth. However, the dependence is very weak, as is supported by the results in Fig. 2, where the maximum and minimum positioning errors over all the azimuth (or θ_x and θ_y) are almost identical. Thus, it is clear that the positioning error is mainly dependent on the elevation, and the azimuth has a negligible impact. Therefore, we only need to optimize the positioning error over elevation in practice. Here the elevation is dependent on the orientation of the antenna array at the BS and the vehicle's position. Therefore an intuitive strategy is to maximize the minimum elevation for all the possible positions in the covered area. This would be possible if we have the map of the target area. Another more intuitive, but less elegant way to understand this result can be found in Appendix A.

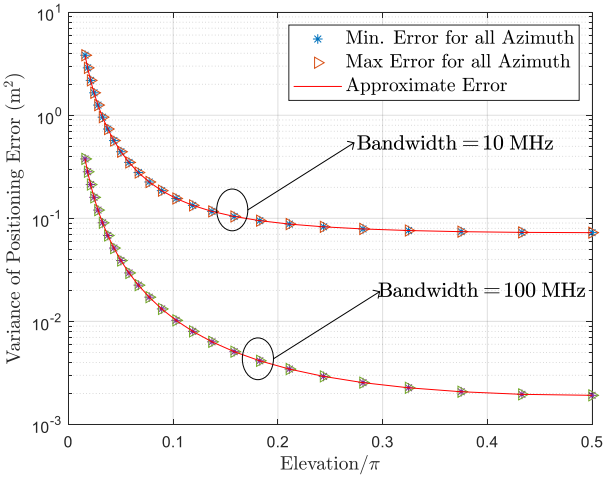

Fig. 2: Impacts of elevation and azimuth on positioning accuracy.

D. The Beam Squint and Doppler Effects

As we have mentioned previously, the beam squint was a challenge in mmWave communications, but it plays a different role in positioning. Similar to [40], we can easily show that the beam squint will actually help to improve the estimation accuracy of AoA, and thus lead to higher positioning accuracy. Specifically, by ignoring the beam squint effect, we can replace

$\mathbf{A}$, $\mathbf{B}$ and $\mathbf{C}$ in (29) with $\mathbf{A}_N$, $\mathbf{B}_N$, $\mathbf{C}_N$, respectively:

$$\begin{aligned}
\mathbf{A}_N =& \frac{2\sigma_a^2 N_x N_y N_t N_s}{\sigma^4} \begin{bmatrix} \overline{n_s^2} & \bar{n}_s\bar{n}_x & \bar{n}_s\bar{n}_y \\ \bar{n}_s\bar{n}_x & \overline{n_x^2} & \bar{n}_x\bar{n}_y \\ \bar{n}_s\bar{n}_y & \bar{n}_x\bar{n}_y & \overline{n_y^2} \end{bmatrix}, \\
\mathbf{B}_N =& \frac{2\sigma_a^2 N_x N_y N_t N_s}{\sigma^4 f_c} \begin{bmatrix} \bar{n}_t\bar{n}_s f_c & \bar{n}_s & 0 \\ \bar{n}_t\bar{n}_x f_c & \bar{n}_x & 0 \\ \bar{n}_t\bar{n}_y f_c & \bar{n}_y f_c & 0 \end{bmatrix}, \\
\mathbf{C}_N =& \frac{2\sigma_a^2 N_x N_y N_t N_s}{\sigma^4} \begin{bmatrix} \overline{n_t^2} f_c^2 & \bar{n}_t f_c & 0 \\ \bar{n}_t f_c & 1 & 0 \\ 0 & 0 & 1/\alpha^2 \end{bmatrix}.
\end{aligned} \tag{39}$$

It can be easily shown that the CRLB of $\mathbf{x}_0$ will increase if we ignore the beam squint effect. The reason is that the beam squint leads to improved AoA estimation accuracy [40]. The improvement is dependent on the total bandwidth, and larger bandwidth leads to more significant beam squint and higher AoA estimation accuracy, given that we can resolve the phase ambiguity. However, even for small bandwidth, if we ignore the beam squint in positioning, it can cause significant performance loss, as we can see from the preliminary numerical results in Fig. 3 and also system-level simulations in next section.

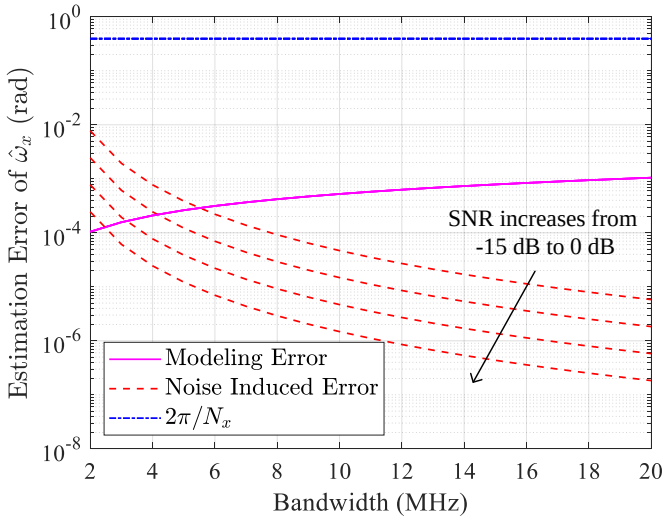

Fig. 3: The impacts of beam squint and noise on estimation accuracy of spatial signature. The simulation results are presented for SNR ranging from -15 dB to 0 dB, with a step of 5 dB.

As we know, the estimation error of spatial signature mainly comes from two sources, the measurement noise and the beam squint, indicated by "Noise Induced Error" and "Modeling Error" respectively. The beam squint can be ignored when its impact is outweighted by that of noise and much smaller than the spatial resolution. Fig. 3 compares the impacts of noise and beam squint for varying bandwidth and SNR. We take ω_x as example with $N_x = 16$, and the spatial resolution is $2\pi/N_s$. From this figure, we can see that the impact of beam squint growes over bandwidth, while the impact of noise declines over both bandwidth and SNR. Even for a relatively small bandwidth of 4 MHz, the beam squint should still be considered.

As for Doppler effect, the measured ω_t is a function of the vehicle's position and velocity. If we don't have any prior information concerning the vehicle's velocity, the Doppler shift will not contribute to positioning accuracy. Fortunately, the speed of the vehicle can be accurately measured at the vehicle side, and the BS has access to accurate map information. When a vehicle moves on a road, the BS can derive the vehicle's 3D velocity, given the vehicle's rough position and speed. This is especially true for railway systems. Therefore, we consider the scenario where $\mathbf{v}$ is known. In such cases, we want to quantify how much more position information can be extracted from the Doppler shift measurements, i.e., ω_t.

With velocity information, the unknown vector will be $\tilde{\boldsymbol{\eta}} = [\mathbf{x}_0^T, \phi_0, \alpha]^T$. The FIM of $\tilde{\boldsymbol{\eta}}$ will be

$$\mathbf{F}_{\tilde{\boldsymbol{\eta}}} = \nabla_{\tilde{\boldsymbol{\eta}}}^T \boldsymbol{\theta} \mathbf{F}_{\boldsymbol{\theta}} \nabla_{\tilde{\boldsymbol{\eta}}} \boldsymbol{\theta}. \tag{40}$$

The Jacobian is given as

$$\nabla_{\tilde{\boldsymbol{\eta}}} \boldsymbol{\theta} = \begin{bmatrix} \mathbf{P} & \mathbf{0} \\ \nabla_{\mathbf{x}_0}^T \omega_t & \mathbf{0} \\ \mathbf{0} & \mathbf{I}_2 \end{bmatrix}. \tag{41}$$

Recall that $v_r = \mathbf{x}_0^T \mathbf{v}/d_0$ and $\omega_t = 2\pi v_r/B/c$, and we have the partial derivatives of ω_t with respect to $\mathbf{x}_0$ given as

$$\nabla_{\mathbf{x}_0} \omega_t = \frac{2\pi}{Bc} \nabla_{\mathbf{x}_0} v_r = \frac{2\pi}{Bc} \left(\frac{\mathbf{v}}{d_0} - \frac{\mathbf{x}_0^T \mathbf{v}}{d_0^3} \mathbf{x}_0 \right). \tag{42}$$

Intuitively, better accuracy should be achieved by considering the Doppler shift measurements. Mathematically, we can easily prove

$$\mathbf{F}_{\tilde{\boldsymbol{\eta}}}^{-1}[1:3, 1:3] \preceq \mathbf{F}_{\boldsymbol{\eta}}^{-1}[1:3, 1:3], \tag{43}$$

which means the lower bound of positioning error is reduced with the additional information. As a result, we can conclude that the Doppler shift will help to improve the positioning accuracy when the vehicle's speed and road map are available.

Through the discussions in this section, we now understand how different system parameters contribute to positioning accuracy. Some of these parameters are not very important for communications, but have huge impacts on localization performance, such as the orientation of the antenna array at the BS. In the following section, we will present low-complexity algorithms to extract the position information from the CSI.

V. Low-Complexity Positioning

In this section, we will present the algorithms for positioning. Suppose the LS channel estimate has already been obtained on specific time slots and sub-carriers, and the estimated CSI is contaminated by noise. At this point, there are two possible choices to extract the position information from the CSI. The first approach is the DPD, where we directly estimate the target's position information from the CSI. Suppose the estimated channel matrix on the n_t-th time slot and n_s-th sub-carrier is $\hat{\mathbf{H}}_{n_t,n_s}$. The channel response is apparently a function of $\boldsymbol{\eta} = [\mathbf{x}_0^T, v_r, \phi_0, \alpha]^T$, i.e., $\mathbf{H}_{n_t,n_s}(\boldsymbol{\eta})$.

The the maximum likelihood estimate of the device's position can be obtained by solving the following problem:

$$\min_{\boldsymbol{\eta}} \sum_{n_t,n_s} \left\| \hat{\mathbf{H}}_{n_t,n_s} - \mathbf{H}_{n_t,n_s}(\boldsymbol{\eta}) \right\|_F^2. \tag{44}$$

We need to conduct a six-dimensional grid search of the optimal solution, which means very high complexity. The second approach is the conventional two-step localization algorithm. The first step is to estimate the position-related parameters from the CSI, including AoA, ToA, and Doppler shift. The second step is to extract position information from these estimated parameters geometrically. The second approach is obviously sub-optimal, and information loss is inevitable. However, note that the communication systems work on medium to high SNR regime, where the information loss is negligible. We will see that the positioning error of the sub-optimal solution is already very close to the CRLB.

Conventionally, there are two popular ways to estimate the position-related parameters from the CSI. The first one is ESPRIT, but it only works well for narrow-band systems. The second one is sparse Bayesian learning (SBL) [42], [43], which is very computationally intensive. Besides, SBL generally fails to approach the CRLB in low to mediu SNR regime, and accurate estimate of SNR is necessary [40]. In this section, we will propose a simple algorithm that has comparable performance to the SBL-based method, with much lower complexity. The estimated parameters will then be utilized for localization through the weighted least squares algorithm.

A. AoA Estimation with Beam Squint

To start with, we conduct channel estimation on the n_t-th time slot and n_s-th sub-carrier, and the LS estimate of $\mathbf{H}_{n_t,n_s}$ can be obtained as $\hat{\mathbf{H}}_{n_t,n_s}$, contaminated by noise. Recall that $\mathbf{H}_{n_t,n_s} = \alpha_{n_t,n_s}\mathbf{a}_{N_x}(\omega_{x,n_s})\mathbf{a}_{N_y}^T(\omega_{y,n_s})$ has three important parameters: ω_{x,n_s}, ω_{y,n_s} and the complex gain α_{n_t,n_s}. Then we can jointly estimate these three parameters by revising the algorithm proposed in [25], and the revised algorithm is summarized in Appendix B for easy reference[2] Suppose ω_{x,n_s} and ω_{y,n_s} are estimated as $\hat{\omega}_{x,n_s}$ and $\hat{\omega}_{y,n_s}$, respectively, and the estimation error follows zero-mean Gaussian distribution [44]. In this case, we have

$$\begin{aligned} \hat{\omega}_{x,n_s} &= \text{wrap}(\omega_x f_{n_s}/f_c + \epsilon_{x,n_s}), \\ \hat{\omega}_{y,n_s} &= \text{wrap}(\omega_y f_{n_s}/f_c + \epsilon_{y,n_s}), \end{aligned} \tag{45}$$

where the $\text{wrap}(\theta)$ maps θ to $[-\pi,\pi)$ with an integer multiple of 2π, while ϵ_{x,n_s}'s and ϵ_{y,n_s}'s are the estimation errors. Notice that small ϵ_{x,n_s}'s and ϵ_{y,n_s}'s can lead to a bias of $\pm 2\pi$. This ambiguity is harmless for communications, but lethal for localization. We will need to estimate ω_x and ω_y based on these biased estimates. In the following discussions, we will present the algorithm for the AoA estimation in the x-direction, and same algorithm can be applied to the y-direction.

In the ideal case, there is a one-to-one relation between ω_{x,n_s} and θ_x. As a result, we can estimate $\cos\theta_x$ through ω_{x,n_s}'s for $n_s \in \{0,1,\cdots,N_s-1\}$. However, the antenna spacing is generally equal to half the carrier wavelength in practice, i.e., $D = \lambda_c/2$, which leads to phase ambiguity on some sub-carriers. To see this, taking ω_{x,n_s} as example, we actually have

$$\hat{\omega}_{x,n_s} = \begin{cases} \omega_x f_{n_s}/f_c + \epsilon_{x,n_s} - 2\pi, & \omega_x f_{n_s}/f_c + \epsilon_{x,n_s} \geq \pi \\ \omega_x f_{n_s}/f_c + \epsilon_{x,n_s} + 2\pi, & \omega_x f_{n_s}/f_c + \epsilon_{x,n_s} < -\pi \\ \omega_x f_{n_s}/f_c + \epsilon_{x,n_s}, & \text{otherwise} \end{cases} \tag{46}$$

This is apparently a piece-wise linear function, and our target is to estimate ω_x. Depending on the value of ω_x, there are three possible cases, as shown in Fig. 4. We will analyze these three cases individually.

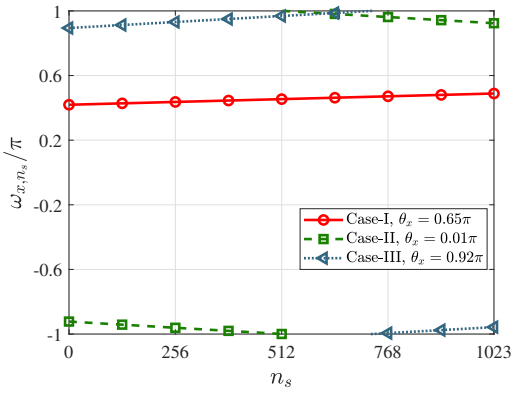

Fig. 4: Three typical cases for different θ_x values.

1) Case-I: Suppose we have $\theta_x = 0.65\pi$, leading to $\omega_x = 0.908\pi$. As a result, we have $\omega_{x,n_s} \in (-\pi,\pi)$ for all sub-carriers, and there is not phase ambiguity. It can be easily shown that the estimation errors on different sub-carriers are i.i.d. Gaussian random variables for reasonable SNR. Thus, the maximum likelihood estimate of ω_x can be obtained by solving the following convex optimization problem:

$$\hat{\omega}_x^{(1)} = \arg\min \sum_{n_s=0}^{N_s-1} |\hat{\omega}_{x,n_s} - \omega_x f_{n_s}/f_c|^2. \tag{47}$$

It is well known that we can get the optimal solution of (47) through the LS estimator as

$$\hat{\omega}_x^{(1)} = (\mathbf{f}^T\mathbf{f})^{-1}\mathbf{f}^T\boldsymbol{\omega}_x, \tag{48}$$

with $\hat{\boldsymbol{\omega}}_x$ and $\mathbf{f}$ given by

$$\begin{aligned} \hat{\boldsymbol{\omega}}_x &= [\hat{\omega}_{x,0}, \hat{\omega}_{x,1}, \cdots, \hat{\omega}_{x,N_s-1}]^T, \\ \mathbf{f} &= \frac{1}{f_c}[f_0, f_1, \cdots, f_{N_s-1}]^T. \end{aligned} \tag{49}$$

2) Case-II: Suppose $\theta_x = 0.01\pi$, and $\omega_x = -0.95\pi$. Because ω_x is very close to $-\pi$, $\omega_x f_{n_s}/f_c$ can be smaller than $-\pi$ for some sub-carriers. Those values smaller than $-\pi$ will be mapped to $(0,\pi)$. As a result, we need to subtract 2π from those positive values to bring them back to where they were:

$$\breve{\omega}_{x,n_s} = \begin{cases} \hat{\omega}_{x,n_s} - 2\pi, & \hat{\omega}_{x,n_s} > 0 \\ \hat{\omega}_{x,n_s}, & \hat{\omega}_{x,n_s} \leq 0. \end{cases} \tag{50}$$

[2]The original algorithm in [25] can estimate ω_{x,n_s} and ω_{y,n_s} jointly. The summary in the appendix is based on a one dimensional case, but it can be easily extended to 2D applications.

Then the LS estimate is given as

$$\hat{\omega}_x^{(2)} = (\mathbf{f}^T\mathbf{f})^{-1}\mathbf{f}^T\breve{\boldsymbol{\omega}}_x, \tag{51}$$

where $\breve{\boldsymbol{\omega}}_x = [\breve{\omega}_{x,0}, \breve{\omega}_{x,1}, \cdots, \breve{\omega}_{x,N_s-1}]^T$.

3) Case-III: Consider $\theta_x = 0.92\pi$, which means $\omega_x = 0.95\pi$. Because ω_x is very close to π, $\omega_x f_{n_s}/f_c$ can be larger than π for some sub-carriers. Those values larger than π will be wrapped to $(-\pi, 0)$. Therefore, we will need to add 2π to those values to drag them back. Specifically, we can unwrap the phase measurements as

$$\breve{\omega}_{x,n_s} = \begin{cases} \hat{\omega}_{x,n_s} + 2\pi, & \hat{\omega}_{x,n_s} < 0 \\ \hat{\omega}_{x,n_s}, & \hat{\omega}_{x,n_s} > 0. \end{cases} \tag{52}$$

Then the LS estimate can be obtained as

$$\hat{\omega}_x^{(3)} = (\mathbf{f}^T\mathbf{f})^{-1}\mathbf{f}^T\breve{\boldsymbol{\omega}}_x. \tag{53}$$

In practice, each case is possible and we will try all of them and find the one that fits the observed data best. The first step is to estimate ω_x through (48), (51), (53), respectively. Then we test each of them based on the observed data, and choose the one with the minimum fitting error, i.e., the maximum likelihood estimate of ω_x will be

$$\hat{\omega}_x = \arg\min_{\hat{\omega}_x^{(n)}} \sum_{n_s} \left| \mathrm{mod}_{2\pi}\left(\hat{\omega}_x^{(n)} f_{n_s}/f_c - \hat{\omega}_{x,n_s}\right)\right|^2. \tag{54}$$

From the above discussions, we understand how ω_x and ω_y can be estimated based on the CSI in one time slot. In practice, if multiple time slots are employed for channel estimation, we can take the average to further reduce the estimation error. The reason for this is that the AoA is almost constant across multiple time slots in one data frame.

B. Estimation of Doppler Shift and Propagation Delay

During the AoA estimation in the previous section, we can simultaneously estimate the complex channel gain α_{n_t,n_s} as $\hat{\alpha}_{n_t,n_s}$. As we can see in (9), the complex channel gain is related to the propagation delay and Doppler shift, i.e., ω_s and ω_{t,n_s}. In this section, we will talk about how to estimate these two parameters from the measured channel gains.

To start with, we estimate ω_{t,n_s} on each sub-carrier. On the n_s-th sub-carrier, the channel gain changes over time slots and we construct the following vector:

$$\boldsymbol{\alpha}_{n_s} = [\alpha_{0,n_s}, \alpha_{1,n_s}, \cdots, \alpha_{N_t-1,n_s}]^T = \alpha_{n_s}\mathbf{a}_{N_t}(\omega_{t,n_s}), \tag{55}$$

with $\alpha_{n_s} = \alpha e^{-j(n_s\omega_s+\phi_0)}$. $\boldsymbol{\alpha}_{n_s}$ is a scaled steering vector, and we can jointly estimate α_{n_s} and ω_{t,n_s} with the algorithm in Appendix B. Suppose ω_{t,n_s} is estimated as

$$\hat{\omega}_{t,n_s} = f_{n_s}\omega_t + \epsilon_{t,n_s}, \tag{56}$$

where ϵ_{t,n_s} is the estimation error. With $\hat{\boldsymbol{\omega}}_t = [\hat{\omega}_{t,0}, \hat{\omega}_{t,1}, \cdots, \hat{\omega}_{t,N_s-1}]^T$ and $\mathbf{f} = [f_0, f_1, \cdots, f_{N_s-1}]^T$, we can get the LS estimate of ω_t as

$$\hat{\omega}_t = (\mathbf{f}^T\mathbf{f})^{-1}\mathbf{f}^T\hat{\boldsymbol{\omega}}_t. \tag{57}$$

Note that we don't need to worry about the phase wrapping issue here, because ω_{t,n_s}'s are very small. The radial velocity is thus estimated as

$$\hat{v}_r = \hat{\omega}_t\frac{Bc}{2\pi}. \tag{58}$$

Meanwhile, we can estimate the complex gain on the n_s-th sub-carrier as

$$\hat{\alpha}_{n_s} = \alpha\exp(-j(n_s\omega_s + \phi_0)) + \epsilon_{n_s}, \tag{59}$$

with ϵ_{n_s} being the estimation error. Putting all the $\hat{\alpha}_{n_s}$'s together, we can see that there is a constant phase shift of ω_s between adjacent sub-carriers. Again, we can use the algorithm in Appendix B to estimate ω_s. Suppose ω_s is estimated as $\hat{\omega}_s$, and the distance between transmitter and receiver will be approximately

$$\hat{d}_0 = \frac{\hat{\omega}_s c}{2\pi B}.$$

C. Positioning Algorithm Design

From the previous discussions, we talked about how to estimate the radial velocity, AoA, and propagation delay from the CSI. With these parameters, we can estimate the mobile device's 3D position. Depending on whether we have map information or not, the Doppler shift measurements may or may not help to improve positioning accuracy. Therefore, we will analyze these two cases individually.

Without map, only ω_s, ω_x and ω_y will be used in positioning. As a result, we would estimate a position that fits the estimated channel parameters well, i.e., minimizing the sum of squared errors. Meanwhile, we should give different parameters different weights, because they have drastically different estimation errors, i.e., weighted least squares (WLS). Suppose the estimated geometrical channel parameters are $\hat{\omega}_s$, $\hat{\omega}_x$ and $\hat{\omega}_y$, the WSL estimate of vehicle's position will be the solution of the following problem:

$$\begin{aligned} \min_{\mathbf{x}_0} \ & \frac{|\omega_s(\mathbf{x}_0) - \hat{\omega}_s|^2}{\sigma_{\omega_s}^2} + \frac{|\omega_x(\mathbf{x}_0) - \hat{\omega}_x|^2}{\sigma_{\omega_x}^2} + \frac{|\omega_y(\mathbf{x}_0) - \hat{\omega}_y|^2}{\sigma_{\omega_y}^2} \\ \text{s.t. } & z > 0, \end{aligned} \tag{60}$$

with $\omega_x(\mathbf{x}_0) = -\pi x/d_0$, $\omega_y(\mathbf{x}_0) = -\pi y/d_0$, $\omega_s(\mathbf{x}_0) = 2\pi B d_0/c$. A problem here is how can we get $\sigma_{\omega_s}^2$, $\sigma_{\omega_x}^2$, $\sigma_{\omega_y}^2$, i.e., the estimation errors of ω_s, ω_x, ω_y respectively. One possible solution is to use the CRLB we derived to approximate these estimation errors, which is very accurate for medium to high SNR regime. However, a problem still remains: we need to know the vehicle's position to compute the CRLB[3]. In practice, we can use the positioning result of the vehicle from the previous data frames, i.e., tracking results, because one frame is very short and the vehicle's position won't change significantly.

In this formulation, we have a constraint that states $z > 0$, so as to resolve the ambiguity of planar arrays. Specifically, if $\mathbf{x}^* = [x^*, y^*, z^*]^T$ can minimize the cost function in (60),

[3]The SNR is also needed, but it is not a problem because all these three variances are inversely proportional to the SNR, and we only cares about the relative weights.

$\tilde{\mathbf{x}}^* = [x^*, y^*, -z^*]^T$ will be an equally good solution. To eliminate the ambiguity, we add the constraint $z > 0$. This problem can be solved iteratively, and we can speed up the convergence by choosing a proper initial value. A good initial estimate can be easily obtained as:

$$\hat{d}_0 = \frac{\hat{\omega}_s c}{2\pi B}, \hat{x} = -\frac{\hat{\omega}_x \hat{d}_0}{\pi}, \hat{y} = -\frac{\hat{\omega}_y \hat{d}_0}{\pi}, \hat{z} = \sqrt{\hat{d}_0^2 - \hat{x}^2 - \hat{y}^2}. \tag{61}$$

Then we solve the optimization problem in (60) iteratively with Newton's method. In this case, we can also estimate the tangential velocity, which indicates how fast Doppler shift varies. This value might be used for vehicle tracking between frames, but it won't directly contribute to positioning accuracy in a given data frame.

Suppose the vehicles can report their real-time velocity, and we have the map information. Then the BS will be able to utilize that information, and the optimization problem is reformulated as

$$\begin{aligned} &\min_{\mathbf{x}_0} \ f(\mathbf{x}_0) \\ &\text{s.t. } z > 0. \end{aligned} \tag{62}$$

$f(\mathbf{x}_0)$ is given as

$$\begin{aligned} f(\mathbf{x}_0) = &\frac{|\omega_s(\mathbf{x}_0) - \hat{\omega}_s|^2}{\sigma_{\omega_s}^2} + \frac{|\omega_x(\mathbf{x}_0) - \hat{\omega}_x|^2}{\sigma_{\omega_x}^2} + \\ &\frac{|\omega_y(\mathbf{x}_0) - \hat{\omega}_y|^2}{\sigma_{\omega_y}^2} + \frac{|\omega_t(\mathbf{x}_0) - \hat{\omega}_t|^2}{\sigma_{\omega_t}^2}, \end{aligned} \tag{63}$$

with $\omega_t(\mathbf{x}_0) = 2\pi \mathbf{x}_0^T \mathbf{v}/d_0/B/c$. Similarly, we can employ (61) to get initial estimate, and then solve the optimization problem iteratively.

Generally, the channel estimation is conducted in each frame/sub-frame in MIMO-OFDM systems. For example, in LTE one sub-frame has a duration of 0.5 ms, and CSI is updated very fast. After each channel estimation, the positioning algorithm will be able to extract the real-time position of the vehicle based on the CSI. Therefore, the position update frequency is very high, at the level of hundreds of Hertz.

D. Complexity Analysis

For high-speed vehicles, the timeliness of the positioning algorithm is as important as accuracy. In this section, we will thoroughly analyze the computational complexity of the SLAC system. Based on the estimated CSI, we can roughly divide the positioning process into two major steps: (a) the estimation of geometrical channel parameters, (b) the localization algorithm. The complexity of step (b) is negligible, because the iterative algorithm used to solve the localization problem in (60) or (63) only involves multiplication and inversion of small matrixes and vectors. Besides, with proper initial estimate, the algorithm will generally converge in two or three iterations. Therefore, we will focus on the analysis of step (a).

There are four geometrical channel parameters to estimate, two AoAs (θ_x and θ_y), propagation delay, and Doppler shift. For estimation of θ_x, the major complexity comes from the Fourier transform. For every sub-array in the x-direction, the complexity is $\mathcal{O}(N_x \log(N_x)$[4] and we have N_y such sub-arrays in total. The overall complexity is thus $\mathcal{O}(N_x N_y \log N_x)$. Similarly, the estimation of θ_y involves a complexity of $\mathcal{O}(N_x N_y \log N_y)$. The signal processing complexity for a given time slot and sub-carrier is $\mathcal{O}(N_x N_y (\log N_x + \log N_y))$. Because this has to be done on each sub-carrier and time slot, the overall complexity will increase by a factor of $N_t N_s$. Consider the beam squint, we need to combine the measurements from all the sub-carriers and solve the problem in (54), with a complexity of $\mathcal{O}(N_s)$. At this point, we already transformed the signal to beamspace, and we will only focus on the strongest component in space. The signal dimension is reduced from $N_x \times N_y \times N_t \times N_s$ to $N_t \times N_s$. Then, we need to estimate ω_t through the FFT algorithm, and on each sub-carrier the complexity of estimating ω_{t,n_s} is $\mathcal{O}(N_t \log N_t)$, leading to a total complexity of $N_s N_t \log N_t$. The last step is to estimate the propagation delay, with a complexity of $\mathcal{O}(N_s \log N_s)$. These analyses are briefly summarized in Table II.

TABLE II: Computational Complexity

Estimate of θ_x	$\mathcal{O}(N_t N_s N_x N_y \log N_x)$
Estimate of θ_y	$\mathcal{O}(N_t N_s N_x N_y \log N_y)$
Estimation of ω_t	$N_s N_t \log N_t$
Estimation of ω_t	$N_s \log N_s$

Overall, the computational complexity grows almost linearly with the number of antennas, frame length and number of sub-carriers. If these four geometrical channel parameters are estimated jointly, the complexity is very high due to the four-dimension search. However, we are sequentially estimating these four parameters in our case without introducing noticable information loss. The reason is that the phase shifts over space, time and frequency are not coupled. The computational complexity of AoA estimation dominates, while that of Doppler shift or delay estimation is much lower.

VI. Numerical Evaluations

In this section, we will conduct simulations to verify the presented analyses and algorithms. Specifically, we will show that the proposed algorithm can provide very accurate position estimate in reasonable SNR range. The carrier frequency is 30 GHz, with 16×16 antennas at the BS and a sub-carrier spacing of 1 MHz. Consider high-speed railway systems, with a train moving at 360 km/h, or 100 m/s equivalently. QPSK modulation is employed throughout the simulations.

A. Estimation of AoA, Propagation Delay, and Doppler Shift

Accurate estimation of AoA, propagation delay and Doppler shift is apparently very important for localization. For wideband mmWave communications, the spatial wideband effect is generally ignored in SLAC, which will deteriorate estimation accuracy of AoA. For every sub-carrier, we will first estimate the spatial signatures on different sub-carriers individually, which is a necessary step for both the conventional work and our work. This is a classic problem and many algorithms have

[4] $\log(x)$ gives the base-2 logarithm of x.

been developed. We will use the algorithm presented in Appendix B due to the low-complexity and great performance in medium to high SNR regime. When beam squint is considered, we know that the spatial signatures on different sub-carriers are piece-wise linear with respect to the sub-carrier index, and we can estimate AoAs by solving the optimization problem in (54). As comparison, if the beam squint is ignored we can directly take the average of estimated spatial signatures on different sub-carriers. Besides, because the Doppler shift is estimated after the AoA, the estimation error in AoA will propagate into Doppler shift estimate. Thus, the spatial wideband effect will not only reduce AoA estimation accuracy, but also that of Doppler shift, as we can see in Fig. 5.

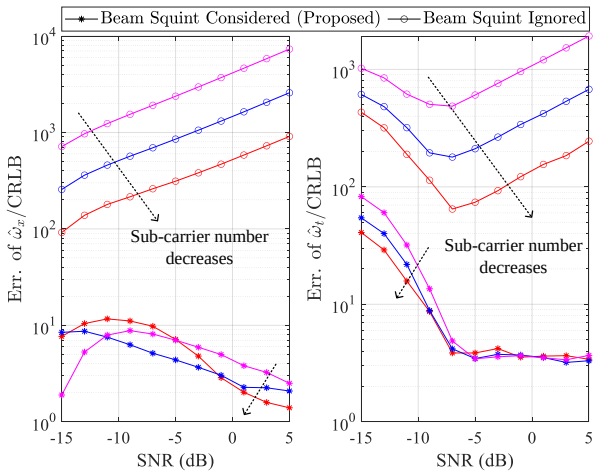

Fig. 5: Estimation error of AoA and Doppler shift with beam squint.

In Fig. 5, the y-axis denotes the ratio of estimation error to the CRLB. We increase the number of sub-carriers from 100 to 200 and then to 400. For the conventional SLAC models, the estimation error will increase, because the beam squint effect becomes stronger as we increase the total bandwidth. Besides, the ratio of estimation error to CRLB will increase when we boost the SNR. This can be explained by the fact that the estimation error is caused by both the noise and the spatial wideband effect. As SNR increases, the estimation error caused by spatial wideband effect will gradually dominate and it will be more loudly pronounced. Similar phenomenon can be observed on velocity estimation error. For low SNR, the noise dominates and the estimation error decreases as we increase SNR. When the SNR is high enough, the spatial wideband effect will dominate and the relative estimation error will increase. For the proposed method, the ratio will gradually decrease, and eventually level off at high SNR.

B. Positioning Accuracy with Beam Squint

In this part, we compare the positioning accuracy of the proposed method, CRLB, and that based on the conventional channel model. For now, we will assume no map is available, and we cannot utilize the Doppler shift measurements for better accuracy. By doing so, we can observe how the beam squint contributes to positioning accuracy. For this part, the bandwidth is a very important parameter. As the number of sub-carriers increases, the CRLB will decrease. The proposed method can closely approach the CRLB, and benefits from the increased bandwidth. However, if the spatial wideband effect is ignored, the positioning accuracy will significantly decrease. For the conventional model with beam squint ignored, the performance will deteriorate as the bandwidth increases, because the spatial wideband effect becomes more severe.

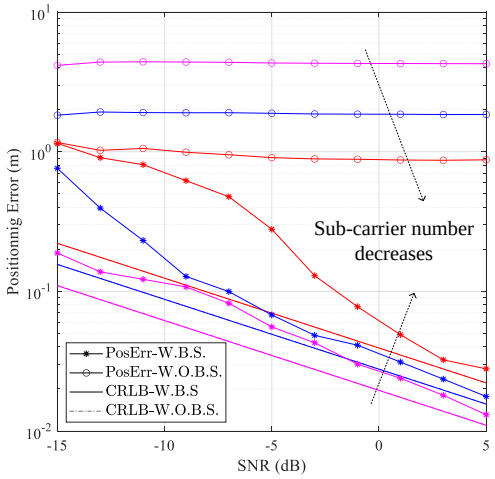

Fig. 6: Positioning error with or without considering beam squint.

We can observe a performance gap between CRLB and the proposed low-complexity algorithm. At low SNR with relatively small bandwidth, the gap is not small, but the positioning error is still at the same order of magnitude with CRLB. However, this gap will gradually vanish with the increase of SNR. A very interesting observation is that the positioning accuracy will stay the same for different SNRs if the beam squint is ignored. This is because the parameter estimation error is mainly dependent on the modeling error resulting from the beam squint, and the noise-induced estimation error can be ignored in high SNR regime.

C. Positioning Accuracy with Doppler Shift

With enough prior information, i.e., map of the target area and speed of the vehicle, we will be able to improve the positioning accuracy by taking the Doppler shift measurements into consideration. As we can see in Fig. 7, the positioning errors are presented when frame length varies from 64 symbols to 128 and then to 256. For short frame length, the positioning errors with or without Doppler shift measurements are almost identical. As the frame length increases, the contribution of Doppler shift will become more significant. This is because the increased frame length allows us to accurately estimate the Doppler shift (or angle of departure, equivalently), leading to higher frequency resolution (or spatial resolution, equivalently) and positioning accuracy. In the right hand side of Fig. 7, we depicted the potential accuracy improvement that is expected from the CRLB analysis, and the actual gain we obtained. The potential gain is obtained by comparing the CRLBs of localization error with and without the Doppler

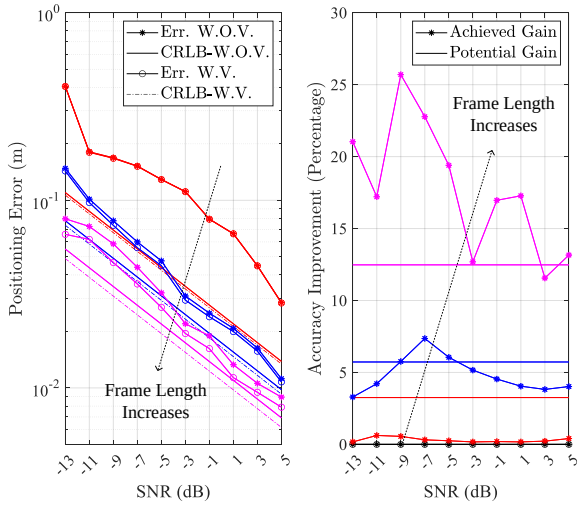

Fig. 7: Positioning error with or without Doppler shift measurements.

shift measurements, while the achieved gain is obtained by comparing the actual localization errors with and without Doppler shift measurements. The CRLB of positioning error without Doppler shift is given by (34) in Section IV.B, while that for the case of incorporating Doppler shift can be easily obtained by taking the inverse of the FIM in (40). For a frame length of 64 symbols, the performance improvement is negligible. However, when we double the frame length, the positioning error can be reduced by around 5 percent. If we further double the frame length again to 256 symbols, the positioning accuracy improvement can be as high as 25 percent for certain SNRs.

Another observation is that the percentage of contribution from Doppler shift measurements is fluctuating over SNR, and it seems that the achieved gain is generally larger for lower SNR, even above the potential gain. In high SNR regime, the Doppler shift estimation error is smaller, but so are the errors of delay and AoA measurements. Therefore, the positioning error based on delay and AoAs is already very small, and the relative contribution of Doppler shift measurements is not necessarily larger. As a matter of fact, we can see that in low SNR regime the contribution from Doppler shift measurements is increasing in percentage. Because the delay and AoAs estimates are not accurate in this case, and the information brought by the Doppler shift measurements is of greater value. This is very much like the left hand side of Fig. 7, where the estimation errors are constantly decreasing when the SNR increases. However, the descending speed changes, and we will also see fluctuation if the error is normalized over SNR. Another interesting point is that the achieved gain can be larger than potential gain. To understand this, note that the potential gain is derived from CRLB, which serves as a lower bound for any unbiased estimators, while the low-complexity algorithm proposed previously is biased, and the bias is more pronounced in low SNR regime.

VII. Conclusions and Future Work

A. Conclusion

In this paper, we discussed various fundamental problems in mmWave-based SLAC for high-mobility single-antenna vehicles and a base station equipped with a massive antenna array. First, we showed that the spatial wideband effect plays a very important role in angle and Doppler shift estimation accuracy. Ignoring this problem will lead to high positioning error. Second, we showed that the Doppler shift measurements also help to improve positioning accuracy, and the improvement is dependent on frame length. With longer frames, Doppler shift measurements contribute more. Third, we simplified the positioning error as a function of the BS antenna array's orientation, and proved that the elevation angle dominates. Therefore, we only need to consider the elevation angle when installing BS antenna arrays. Based on the comprehensive modeling, we derived lower bounds of positioning error and showed that these bounds can be closely achieved with low-complexity algorithms. The underlying idea of the low-complexity algorithm is that we can estimate the geometrical channel parameters sequentially with negligible information loss. By considering the Doppler effect and spatial wideband effect, SLAC can provide centimeter-level accuracy in real-time positioning with reasonable bandwidth, SNR and large antenna array.

B. Future Work

As extension of the current work, an immediate problem is the tracking of mobile devices. That is to say, we need to consider the positioning of mobile devices in multiple continuous frames. In this case, it might be possible to utilize the Doppler shift for positioning even without map information. Second, we already know that multi-path components will not help to improve positioning accuracy if the mobile device has a single antenna. However, if we consider the Doppler effect and the synthesized array, will it be possible to distinguish multiple paths and utilize them for positioning? We already started the investigation of these two issues and we hope to answer them to some extent in the near future.

Appendix A
Inverse of $\mathbf{P}$ and Approximated CRLB

In this appendix, we will talk about the inverse of $\mathbf{P}$ and another more intuitive way to understand the approximation of the CRLB in (37). To start with, we multiply the first row by a factor and move the first row to the last. Thus, $\mathbf{P}$ can be decomposed as

$$\mathbf{P}^T = \frac{\pi}{d_0}\begin{bmatrix} \tilde{x}^2-1 & \tilde{x}\tilde{y} & \tilde{x}\tilde{z} \\ \tilde{x}\tilde{y} & \tilde{y}^2-1 & \tilde{y}\tilde{z} \\ \tilde{x}\tilde{z} & \tilde{y}\tilde{z} & \tilde{z}^2 \end{bmatrix}\begin{bmatrix} 0 & 1 & 0 \\ 0 & 0 & 1 \\ \frac{2Bd_0^2}{cz} & 0 & 0 \end{bmatrix} \tag{64}$$

with $\tilde{x} = x/d_0$, $\tilde{y} = y/d_0$, $\tilde{z} = z/d_0$. By defining $\mathbf{U} = [\tilde{x}, \tilde{y}, \tilde{z}; 0, 0, 1]^T$, and the first matrix on the right hand side can be rewritten as $-\left(\mathbf{I} - \mathbf{U}\mathbf{U}^T\right)$, and its inverse is given by

$$\begin{aligned}\left(\mathbf{I} - \mathbf{U}\mathbf{U}^T\right)^{-1} =& \mathbf{I} + \mathbf{U}\left(\mathbf{I} - \mathbf{U}^T\mathbf{U}\right)^{-1}\mathbf{U}^T \\ =& \mathbf{I} - \frac{1}{\tilde{z}}\mathbf{U}\begin{bmatrix} 0 & 1 \\ 1 & 0 \end{bmatrix}\mathbf{U}^T \\ =& \begin{bmatrix} \mathbf{I}_2 & \mathbf{b} \\ \mathbf{b}^T & -1 \end{bmatrix}.\end{aligned}$$

with $\mathbf{b} = [-x/z, -y/z]^T$. Suppose we already get unbiased estimate of ω_s, ω_x and ω_y, as $\hat{\omega}_s$, $\hat{\omega}_x$ and $\hat{\omega}_y$, while the distance is estimated as $\hat{d}_0$. The coordinate will be approximately computed as (61). Taking the first-order Taylor expansion, we have the estimation errors as

$$\begin{aligned}\delta_x =& \hat{x} - x \approx d_0\delta_{\omega_x}/\pi + \omega_x\delta_{d_0}/\pi, \\ \delta_y =& \hat{y} - y \approx d_0\delta_{\omega_y}/\pi + \omega_y\delta_{d_0}/\pi, \\ \delta_z =& \hat{z} - z \approx \omega_z\delta_{d_0}/\pi - \frac{d_0\omega_x}{\omega_z\pi}\delta_{\omega_x} - \frac{d_0\omega_y}{\omega_z\pi}\delta_{\omega_y}.\end{aligned} \tag{65}$$

The correlations among estimated ω_x, ω_y and ω_t are very weak. Thus, we ignore the correlations and obtain the approximate positioning error at three dimensions as

$$\begin{aligned}\sigma_x^2 =& \mathbb{E}\{\delta_x^2\} \approx \left(d_0^2\sigma_{\omega_x}^2 + \omega_x^2\sigma_{d_0}^2\right)/\pi^2, \\ \sigma_y^2 =& \mathbb{E}\{\delta_y^2\} \approx \left(d_0^2\sigma_{\omega_y}^2 + \omega_y^2\sigma_{d_0}^2\right)/\pi^2, \\ \sigma_z^2 =& \mathbb{E}\{\delta_z^2\} \approx d_0^2\frac{\omega_x^2\sigma_{\omega_x}^2 + \omega_y^2\sigma_{\omega_y}^2}{\omega_z^2}/\pi^2 + \omega_z^2\sigma_{d_0}^2/\pi^2.\end{aligned} \tag{66}$$

The total positioning error is

$$\begin{aligned}\sigma_{\mathbf{x}_0}^2 =& \mathbb{E}\{\delta_x^2 + \delta_y^2 + \delta_z^2\} \\ =& \frac{d_0^2}{\pi^2}\left((1 + \omega_x^2/\omega_z^2)\sigma_{\omega_x}^2 + (1 + \omega_y^2/\omega_z^2)\sigma_{\omega_y}^2\right) + \sigma_{d_0}^2,\end{aligned}$$

which is identical to (37).

Appendix B
DFT-Based Frequency and Complex Gain Estimation

In this section, we talk about the joint estimate of the frequency and complex gain of a complex sinusoid sequence. Suppose the signal sequence is $\mathbf{y}$ of length N, with the n-th element given as

$$\mathbf{y}[n] = \alpha e^{-jn\omega} + w_n, \tag{67}$$

where w_n's are i.i.d. CSCG random variables with a variance of σ^2. Similar to the previous discussions, we assume α is known at the BS (pilot symbol, or data symbol from previous frames in channel tracking). Our goal is to estimate α and ω. [5] By conducting the IDFT on $\mathbf{y}$, we have

$$\begin{aligned}\mathbf{y}_\omega[k] =& \frac{1}{\sqrt{N}}\sum_{n_t=0}^{N-1}\mathbf{y}[n]e^{jnk\omega_0} \\ =& \frac{\alpha}{\sqrt{N}}e^{-j(N-1)(\omega - k\omega_0)/2}\frac{\sin(N(\omega - k\omega_0)/2)}{\sin((\omega - k\omega_0)/2)} + \tilde{\mathbf{w}}[k],\end{aligned} \tag{68}$$

[5] In practice, $\mathbf{y}$ will be the LS estimate of the channel vector/matrix, obtained from the pilot sequence.

with $\omega_0 = 2\pi/N$ and $\tilde{\mathbf{w}}$ being the IDFT of the noise sequence. Suppose $\omega = (l + \beta)\omega_0$, with $l \in \{0, 1, \cdots, N-1\}$ and $\beta \in [0, 1)$. Therefore, we know that

$$|\mathbf{y}_\omega[l]| \approx \frac{|\alpha|\sin(\beta\pi)}{\beta\pi/\sqrt{N}},\ |\mathbf{y}_\omega[l+1]| \approx \frac{|\alpha|\sin(\beta\pi)}{(1-\beta)\pi/\sqrt{N}} \tag{69}$$

Thus, we can estimate β through

$$\hat{\beta} = \frac{|\mathbf{y}_\omega[l+1]|}{|\mathbf{y}_\omega[l]| + |\mathbf{y}_\omega[l+1]|}, \tag{70}$$

leading to the estimate of ω as $\tilde{\omega} = (l + \hat{\beta})\omega_0$. With estimated ω, we can now estimate the complex gain based on the two samples in the main lobe of the spectrum, i.e., $\mathbf{y}_\omega[l]$ and $\mathbf{y}_\omega[l+1]$. In [14], the authors showed that more than 80% of the total energy concentrates on these two samples in the main lobe. As a result, by only using $\mathbf{y}_\omega[l]$ and $\mathbf{y}_\omega[l+1]$ to estimate the complex channel gain, the information loss will be negligible, while the complexity can be significantly reduced. Suppose perfect estimate of β is available, the LS estimate of the complex channel gain is

$$\hat{\alpha} = \frac{b_{l+1}\mathbf{y}_\omega[l] + b_l\mathbf{y}_\omega[l+1]}{|b_l|^2 + |b_{l+1}|^2}, \tag{71}$$

where b_l and b_{l+1} are given as

$$\begin{aligned}b_l =& \sqrt{N}e^{j(N-1)\beta\pi/N}\frac{\sin(\beta\pi)}{\beta\pi}, \\ b_{l+1} =& \sqrt{N}e^{j(N-1)(\beta-1)\pi/N}\frac{\sin(\beta\pi)}{(1-\beta)\pi}.\end{aligned} \tag{72}$$

References

[1] S. Jeong, O. Simeone, and J. Kang, "Optimization of massive full-dimensional MIMO for positioning and communication," *IEEE Transactions on Wireless Communications*, vol. 17, pp. 6205–6217, July 2018.

[2] A. Fascista, A. Coluccia, H. Wymeersch, and G. Seco-Granados, "Millimeter-wave downlink positioning with a single-antenna receiver," *IEEE Transactions on Wireless Communications*, vol. 18, pp. 4479–4490, July 2019.

[3] Z. He, Y. Ma, and R. Tafazolli, "Improved high resolution TOA estimation for OFDM-WLAN based indoor ranging," *IEEE Wireless Communications Letters*, vol. 2, pp. 163–166, Jan. 2013.

[4] R. Di Taranto, S. Muppirisetty, R. Raulefs, D. Slock, T. Svensson, and H. Wymeersch, "Location-aware communications for 5G networks: How location information can improve scalability, latency, and robustness of 5G," *IEEE Signal Processing Magazine*, vol. 31, pp. 102–112, Oct. 2014.

[5] R. Mendrzik, H. Wymeersch, and G. Bauch, "Joint localization and mapping through millimeter wave MIMO in 5G systems," in *2018 IEEE Global Communications Conference (GLOBECOM)*, (Abu Dhabi, United), pp. 1–6, 2018.

[6] Y. Zeng and X. Xu, "Toward environment-aware 6G communications via channel knowledge map," *IEEE Wireless Communications*, vol. 28, pp. 84–91, March 2021.

[7] B. Zhou, A. Liu, and V. Lau, "Successive localization and beamforming in 5G mmWave MIMO communication systems," *IEEE Transactions on Signal Processing*, vol. 67, pp. 1620–1635, Jan. 2019.

[8] Y. Zhao, Z. Li, N. Cheng, B. Hao, and X. Shen, "Joint UAV position and power optimization for accurate regional localization in space-air integrated localization network," *IEEE Internet of Things Journal*, vol. 8, pp. 4841–4854, Oct. 2020.

[9] K. Zheng, H. Wang, H. Li, W. Xiang, L. Lei, J. Qiao, and X. S. Shen, "Energy-efficient localization and tracking of mobile devices in wireless sensor networks," *IEEE Transactions on Vehicular Technology*, vol. 66, pp. 2714–2726, June 2017.

[10] Z.-W. Liu, Z.-H. Guan, X. Shen, and G. Feng, "Consensus of multi-agent networks with aperiodic sampled communication via impulsive algorithms using position-only measurements," *IEEE Transactions on Automatic Control*, vol. 57, pp. 2639–2643, Aug. 2012.

[11] L. Cong and W. Zhuang, "Hybrid TDOA/AOA mobile user location for wideband CDMA cellular systems," *IEEE Transactions on Wireless Communications*, vol. 1, pp. 439–447, July 2002.

[12] X. Li and K. Pahlavan, "Super-resolution TOA estimation with diversity for indoor geolocation," *IEEE Transactions on Wireless Communications*, vol. 3, pp. 224–234, Jan. 2004.

[13] T. Marzetta, "Noncooperative cellular wireless with unlimited numbers of base station antennas," *IEEE Transactions on Wireless Communications*, vol. 9, pp. 3590–3600, Nov. 2010.

[14] Z. Gong, C. Li, and F. Jiang, "Pilot decontamination in noncooperative massive MIMO cellular networks based on spatial filtering," *IEEE Transactions on Wireless Communications*, vol. 18, pp. 1419–1433, Feb. 2019.

[15] H. Wymeersch, D. Shrestha, C. M. de Lima, V. Yajnanarayana, B. Richerzhagen, M. F. Keskin, K. Schindhelm, A. Ramirez, A. Wolfgang, M. F. de Guzman, K. Haneda, T. Svensson, R. Baldemair, and S. Parkvall, "Integration of communication and sensing in 6G: a joint industrial and academic perspective," in *2021 IEEE 32nd Annual International Symposium on Personal, Indoor and Mobile Radio Communications (PIMRC)*, (Helsinki, Finland), pp. 1–7, 2021.

[16] S. Dwivedi, R. Shreevastav, F. Munier, J. Nygren, I. Siomina, Y. Lyazidi, D. Shrestha, G. Lindmark, P. Ernström, E. Stare, S. M. Razavi, S. Muruganathan, G. Masini, A. Busin, and F. Gunnarsson, "Positioning in 5G networks," *IEEE Communications Magazine*, vol. 59, pp. 38–44, Nov. 2021.

[17] S. Wu, N. Zhang, H. Zhou, Q. Zhang, and X. Shen, "High precision ranging with IR-UWB: a compressed sensing approach," *Wirel. Commun. Mob. Comput.*, vol. 16, pp. 3015–3031, Dec. 2016.

[18] T. Wang, Y. Shen, S. Mazuelas, H. Shin, and M. Z. Win, "On OFDM ranging accuracy in multipath channels," *IEEE Systems Journal*, vol. 8, pp. 104–114, Oct. 2014.

[19] N. Garcia, H. Wymeersch, E. G. Larsson, A. M. Haimovich, and M. Coulon, "Direct localization for massive MIMO," *IEEE Transactions on Signal Processing*, vol. 65, pp. 2475–2487, Feb. 2017.

[20] K. Witrisal, P. Meissner, E. Leitinger, Y. Shen, C. Gustafson, F. Tufvesson, K. Haneda, D. Dardari, A. F. Molisch, A. Conti, and M. Z. Win, "High-accuracy localization for assisted living: 5G systems will turn multipath channels from foe to friend," *IEEE Signal Processing Magazine*, vol. 33, pp. 59–70, March 2016.

[21] A. Shahmansoori, G. E. Garcia, G. Destino, G. Seco-Granados, and H. Wymeersch, "Position and orientation estimation through millimeter-wave MIMO in 5G systems," *IEEE Transactions on Wireless Communications*, vol. 17, pp. 1822–1835, Dec. 2017.

[22] A. Shahmansoori, B. Uguen, G. Destino, G. Seco-Granados, and H. Wymeersch, "Tracking position and orientation through millimeter wave lens MIMO in 5G systems," *IEEE Signal Processing Letters*, vol. 26, pp. 1222–1226, July 2019.

[23] A. Fascista, M. F. Keskin, A. Coluccia, H. Wymeersch, and G. Seco-Granados, "RIS-aided joint localization and synchronization with a single-antenna mmWave receiver," *IEEE Journal of Selected Topics in Signal Processing*, vol. 16, pp. 1141–1156, May 2022.

[24] A. Fascista, A. Coluccia, H. Wymeersch, and G. Seco-Granados, "Downlink single-snapshot localization and mapping with a single-antenna receiver," *IEEE Transactions on Wireless Communications*, vol. 20, pp. 4672–4684, March 2021.

[25] Z. Gong, C. Li, F. Jiang, and M. Z. Win, "Data-aided Doppler compensation for high-speed railway communications over mmWave bands," *IEEE Transactions on Wireless Communications*, vol. 20, pp. 520–534, Sep. 2021.

[26] Y. Wang, Y. Wu, and Y. Shen, "Joint spatiotemporal multipath mitigation in large-scale array localization," *IEEE Transactions on Signal Processing*, vol. 67, pp. 783–797, Nov. 2018.

[27] Y. Liu, Y. Shen, and M. Z. Win, "Single-anchor localization and synchronization of full-duplex agents," *IEEE Transactions on Communications*, vol. 67, pp. 2355–2367, Oct. 2018.

[28] F. Ge and Y. Shen, "Single-anchor ultra-wideband localization system using wrapped PDoA," *IEEE Transactions on Mobile Computing*, vol. 21, pp. 4609–4623, May 2022.

[29] M. Giordani, M. Mezzavilla, S. Rangan, and M. Zorzi, "Multi-connectivity in 5G mmWave cellular networks," in *2016 Mediterranean Ad Hoc Networking Workshop (Med-Hoc-Net)*, (Vilanovai la Geltru, Spain), pp. 1–7, 2016.

[30] A. Ravanshid, P. Rost, D. S. Michalopoulos, V. V. Phan, H. Bakker, D. Aziz, S. Tayade, H. D. Schotten, S. Wong, and O. Holland, "Multi-connectivity functional architectures in 5G," in *2016 IEEE International Conference on Communications Workshops (ICC)*, (Kuala Lumpur, Malaysia), pp. 187–192, 2016.

[31] V. Petrov, D. Solomitckii, A. Samuylov, M. A. Lema, M. Gapeyenko, D. Moltchanov, S. Andreev, V. Naumov, K. Samouylov, M. Dohler, and Y. Koucheryavy, "Dynamic multi-connectivity performance in ultra-dense urban mmWave deployments," *IEEE Journal on Selected Areas in Communications*, vol. 35, pp. 2038–2055, June 2017.

[32] M. Drago, T. Azzino, M. Polese, Č. Stefanović, and M. Zorzi, "Reliable video streaming over mmWave with multi connectivity and network coding," in *2018 International Conference on Computing, Networking and Communications (ICNC)*, (Maui, HI, USA), pp. 508–512, 2018.

[33] A. Amar and A. J. Weiss, "Localization of narrowband radio emitters based on Doppler frequency shifts," *IEEE Transactions on Signal Processing*, vol. 56, pp. 5500–5508, Aug. 2008.

[34] A. J. Weiss, "Direct geolocation of wideband emitters based on delay and Doppler," *IEEE Transactions on Signal Processing*, vol. 59, pp. 2513–2521, March 2011.

[35] H. Zhao, N. Zhang, and Y. Shen, "Beamspace direct localization for large-scale antenna array systems," *IEEE Transactions on Signal Processing*, vol. 68, pp. 3529–3544, May 2020.

[36] X. Zheng, A. Liu, and V. Lau, "Joint channel and location estimation of massive MIMO system with phase noise," *IEEE Transactions on Signal Processing*, vol. 68, pp. 2598–2612, April 2020.

[37] F. Jiang, Y. Ge, M. Zhu, and H. Wymeersch, "High-dimensional channel estimation for simultaneous localization and communications," in *2021 IEEE Wireless Communications and Networking Conference (WCNC)*, (Nanjing, China), pp. 1–6, 2021.

[38] Y. Zhao, Z. Li, N. Cheng, W. Wang, C. Li, and X. Shen, "Covert localization in wireless networks: Feasibility and performance analysis," *IEEE Transactions on Wireless Communications*, vol. 19, pp. 6549–6563, June 2020.

[39] B. Wang, F. Gao, S. Jin, H. Lin, and G. Y. Li, "Spatial- and frequency-wideband effects in millimeter-wave massive MIMO systems," *IEEE Transactions on Signal Processing*, vol. 66, pp. 3393–3406, May 2018.

[40] Y. Song, Z. Gong, C. Li, and Y. Chen, "Efficient channel estimation for wideband millimeter wave massive MIMO systems with beam squint," *IEEE Transactions on Communications*, vol. 70, pp. 3421–3435, May 2022.

[41] D. Tse and P. Viswanath, *Fundamentals of wireless communication*. New York: Cambridge University Press, 2005.

[42] M. Jian, F. Gao, Z. Tian, S. Jin, and S. Ma, "Angle-domain aided UL/DL channel estimation for wideband mmWave massive MIMO systems with beam squint," *IEEE Transactions on Wireless Communications*, vol. 18, pp. 3515–3527, May 2019.

[43] Y. Song, Z. Gong, Y. Chen, and C. Li, "Tensor-based sparse Bayesian learning with intra-dimension correlation," *IEEE Transactions on Signal Processing*, vol. 71, pp. 31–46, to appear in 2023.

[44] Z. Gong, C. Li, F. Jiang, and J. Zheng, "AUV-aided localization of underwater acoustic devices based on Doppler shift measurements," *IEEE Transactions on Wireless Communications*, vol. 19, pp. 2226–2239, April 2020.